In Vivo Interaction Proteomics in *Caenorhabditis elegans* Embryos Provides New Insights into P Granule Dynamics*[S]

Jia-Xuan Chen‡§, Patricia G. Cipriani§¶, Desirea Mecenas§, Jolanta Polanowska§‖, Fabio Piano§¶, Kristin C. Gunsalus§¶‡‡, and Matthias Selbach‡‡‡**

Studying protein interactions in whole organisms is fundamental to understanding development. Here, we combine *in vivo* expressed GFP-tagged proteins with quantitative proteomics to identify protein-protein interactions of selected key proteins involved in early *C. elegans* embryogenesis. Co-affinity purification of interaction partners for eight bait proteins resulted in a pilot *in vivo* interaction map of proteins with a focus on early development. Our network reflects known biology and is highly enriched in functionally relevant interactions. To demonstrate the utility of the map, we looked for new regulators of P granule dynamics and found that GEI-12, a novel binding partner of the DYRK family kinase MBK-2, is a key regulator of P granule formation and germline maintenance. Our data corroborate a recently proposed model in which the phosphorylation state of GEI-12 controls P granule dynamics. In addition, we find that GEI-12 also induces granule formation in mammalian cells, suggesting a common regulatory mechanism in worms and humans. Our results show that *in vivo* interaction proteomics provides unique insights into animal development. ***Molecular & Cellular Proteomics 15: 10.1074/mcp.M115.053975, 1642–1657, 2016.***

Protein-protein interactions (PPIs)[1] are central to virtually all aspects of life. The systematic characterization of all PPIs is therefore a major goal and challenge in the post genomic era. Large scale *in vitro* screens using cell lines or the yeast two-hybrid system have generated protein interaction maps that can help to better understand the functional organization of the proteome (1–9). Despite their effectiveness, such *in vitro* experiments cannot reflect all aspects of the complex interplay of proteins from whole organisms or tissues. For example, because proteins are often expressed in a tissue- and stage-dependent manner during the development of a multicellular organism, experiments in cell lines or heterologous systems can result in the identification of interaction partners that are not biologically relevant in a physiologic context. Similarly, many PPIs are regulated by condition-specific post-translational modifications, which may not be adequately represented in yeast or cell-based assay systems. These limitations provide compelling reasons to develop approaches that can capture the endogenous interaction partners of proteins within a living organism.

During embryogenesis, PPIs play key roles in directing and coordinating essential developmental processes. A well-known example is the interaction between the scaffold proteins PAR-3 and PAR-6 with the atypical protein kinase C (aPKC) PKC-3, whose family members are required to establish polarity across the animal kingdom (10, 11). In *C. elegans* embryos, this polarity pathway induces the asymmetric distribution of microscopically visible aggregates of RNAs and proteins, so called P granules. In the one-cell embryo, P granules localize to the posterior and subsequently segregate to the germline progenitor via successive asymmetric cell divisions. Mutations in genes encoding P granule components often cause sterility, indicating that they are key determinants of germ cell identity (12). P granules display liquid-like properties and localize via controlled dissolution and condensation (13). However, the signaling events mediating the dynamics of P granules (and other types of ribonucleoprotein (RNP) granules) are not yet completely understood.

Affinity purification and mass spectrometry (AP-MS) is emerging as a useful technology to map PPIs based on whole

From the ‡Max Delbrück Center for Molecular Medicine, D-13092 Berlin, Germany; §Center for Genomics and Systems Biology, Department of Biology, New York University, New York, NY 10003; ¶New York University Abu Dhabi, Abu Dhabi, United Arab Emirates; ‖INSERM, U1104, 13288 Marseille, France; **Charité-Universitätsmedizin Berlin, 10117 Berlin, Germany.

Received July 30, 2015, and in revised form, February 24, 2016
Published, MCP Papers in Press, February 24, 2016, DOI 10.1074/mcp.M115.053975

Author contributions: JXC, FP, KCG and MS conceived and designed the study. JXC, PGC, DM and JP performed experiments. JXC, PGC, JP, FP, KCG and MS analyzed and interpreted the data. FP, KCG and MS supervised the study. JXC, PGC, FP, KCG and MS wrote the article.

[1] The abbreviations used are: PPI, protein-protein interaction; AP-MS, affinity purification and mass spectrometry; DYRK, dual-specificity tyrosine-regulated kinase; GO, gene ontology; IP, immunoprecipitation; IVI, *in vivo* interactome; LC, low complexity; LCI, literature-curated interactions; LC-MS/MS, liquid chromatography mass spectrometry; LFQ, label-free quantification; RNP, ribonucleoprotein; RNAi, RNA interference; SILAC, stable isotope labelling by amino acids in cell culture; WI8, worm interactome 8.

organisms or tissues. Pioneering work by Cheeseman and co-workers applied this strategy to define interaction partners of kinetochore proteins in *C. elegans* (14, 15). A major challenge in such experiments is the trade-off between sensitivity and specificity. On the one hand, mild purification conditions preserve transient interactions but also lead to a high number of nonspecific contaminants. On the other hand, stringent purification procedures, such as tandem affinity purification (TAP), reduce nonspecific binding but could lead to loss of transient interactions. Most published studies did not employ quantification, which makes it difficult to distinguish genuine interaction partners from nonspecific contaminants (15–18). Quantitative affinity purification and mass spectrometry solves this problem by using quantification as an additional filter (19–21). Here, the abundance of proteins coprecipitating with the bait protein under mild conditions is compared with a suitable control experiment. Specific interaction partners can then be identified by their high abundance ratio. For example, this approach has been used to identify interaction partners of GFP-fusion proteins in tissue culture cells (22). This eliminates the need for extensive purification and greatly increases the confidence in the data. However, so far this was largely limited to the analysis of single bait proteins *in vivo* (23, 24). To our knowledge, the approach has not yet been employed for systematic *in vivo* PPI mapping in *C. elegans* early embryos.

Here, we use mass spectrometry-based quantitative proteomics to identify interaction partners of eight proteins involved in multiple aspects of *C. elegans* early embryogenesis. Our interaction network reflects known biology and is highly enriched in interacting proteins that share related phenotypes and functional annotations. We followed up on the biological role of the novel MBK-2 interaction partner GEI-12 and show that GEI-12 and its paralog are key regulators of P granule assembly. Our results are also supported by a recent report in which MBK-2 was found to phosphorylate GEI-12 *in vitro* and the *in vivo* phosphorylation level of the protein was affected by MBK-2 and PPTR-1 (25). Additionally, we demonstrated that MBK-2 is physically associated with both GEI-12 and PPTR-2 in embryos and that GEI-12 forms RNP granules when expressed in mammalian cells. In summary, our data show that quantitative *in vivo* interaction proteomics provides unique insights into protein function during development.

EXPERIMENTAL PROCEDURES

C. elegans Culture and Strains—*C. elegans* strains were cultured on OP50 seeded NGM plates using standard techniques as previously described (26). SILAC worm culture was performed as reported (27). Briefly, peptone-free NGM plates containing antibiotic-antimycotic (Invitrogen, Carlsbad, CA) were seeded with a lysine-auxotrophic *E. coli* strain AT713 metabolically labeled with either Lys-0: L-lysine-$^{12}C_6{}^{14}N_2$ ('light') or Lys-8: L-lysine-$^{13}C_6{}^{15}N_2$ ('heavy'). Synchronized L1 larvae were added to the seeded plates and grown for one generation.

The following strains and mutants were used in this study: Bristol N2 (wild-type), *gei-12(tm4526)*, *gei-12(tm4259)*, *C36C9.1(tm4343)*, *pptr-1(tm3103)*

BS1080 *ozIs5*[*GLD-1::GFP::FLAG; unc-119(+)*] (28)
EK244 *cmIs6*[*MBK-1::GFP; unc-4(+)*] (29)
JH1576 *axIs1140*[*Ppie-1::GFP::MBK-2; unc-119(+)*] (30)
JH2015 *axIs1462*[*Ppie-1::GFP::PIE-1::3′pie-1; unc-119(+)*] (31)
JH2017 *axIs1464*[*Ppie-1::GFP::PGL-3::3′pgl-3; unc-119(+)*] (31)
JH2166 *axIs1567*[*Ppie-1::GFP::SPN-4::3′spn-4; unc-119(+)*] (31)
JH2688 *axIs1927*[*Ppie-1::LAP::GLH-1::3′nos-2; unc-119(+)*] (32)
MG170 (*zen-4(or153ts) IV; xsEx6*[*ZEN-4::GFP*]) (33)
PF633 *nnIs265*[*Ppie-1::PAR-6::GFP::3′pie-1; unc-119(+)*]
PF720 *nnIs352*[*Ppie-1::POS-1::GFP::3′pie-1; unc-119(+)*]
PF1207 *nnIs795*[*Pgld-1::GEI-12::GFP::3xFLAG::3′unc-54; unc-119(+)*]
SS747 *bnIs1*[*Ppie-1::GFP::PGL-1; unc-119(+)*] (34)
TH120 ([*Ppie-1::GFP::PAR-2::3′par-2*]; [*Ppie-1::mCherry::PAR-6::3′pie-1*]) (35)
WH346 *ojIs34*[*GFP::CAR-1; unc-119(+)*]

Cloning—Full-length gei-12 was amplified from N2 cDNA using the GATEWAY forward primer 5′-GGGGACAAGTTTGTACAAAAAAGCAGGCTTGAGTTCCTCAAAACCTTACCCA-3′ and reverse primer 5′-GGGGACCACTTTGTACAAGAAAGCTGGGTATTGATCTCTGGGTGGGTCAAAAATAG-3′, cloned into the pDONR221 vector and subcloned into pCFJ150 vector (36) for microparticle bombardment and into a pDEST_EGFP destination vector (gift from Markus Landthaler) for mammalian cell expression. For generating the mbk-2 RNAi clone, a 1393 bps genomic fragment of mbk-2 was PCR amplified using forward primer: 5′-CGATCACACACATCCTCGTC-3′ and reverse primer: 5′-AACCTCATGATCGGCAAGTC-3′, TA cloned into the RNAi feeding vector (L4440) and transformed into HT115 bacteria as described (37).

Mammalian Cell Culture and Transfection—HEK293T cells were maintained in a humidified incubator under 5% CO_2 at 37 °C in DMEM medium supplemented with 10% fetal bovine serum and 4 mM GlutaMAX. SILAC cell culture was performed using SILAC DMEM media containing either ("light") Lys-0: L-lysine-$^{12}C_6{}^{14}N_2$, Arg-0: L-arginine-$^{12}C_6{}^{14}N_4$ or ("heavy") Lys-8: L-lysine-$^{13}C_6{}^{15}N_2$, Arg-10: L-arginine-$^{13}C_6{}^{15}N_4$ and supplemented with 10% dialyzed fetal bovine serum, 4 mM GlutaMAX and 1 mM sodium pyruvate. Cells were transfected using standard protocols with linear polyethylenimine (PEI) transfection reagent (Polysciences, Warrington, PA) for pull-down experiments and with Lipofectamine 2000 (Invitrogen) for fluorescence microscopy.

RNAi and Sterility Assays—Feeding RNAi was performed similar to previously described (38). Briefly, inoculated RNAi bacterial culture was grown in LB media containing 50 μg/ml ampicillin for ~7 h, followed by IPTG (1 mM) induction for 1 h. The bacterial culture was then seeded onto NGM plates containing 50 μg/ml ampicillin and 1 mM IPTG. Seeded plates were let dry, protected from light and incubated at room temperature overnight. Synchronized L1 larvae were then added to the seeded plates and were incubated at 25 °C for ~48 h until F1 embryos could be harvested for further examinations.

For trans-generational feeding and sterility assays, L1 larvae were subjected to *gei-12(RNAi)* continuously through adulthood on solid medium at 15 °C or 25 °C; multiple L1 progeny were individually transferred to new feeding plates and the process was repeated through two filial generations. Adults from each generation were examined individually and scored as sterile if no embryos were visible in the uterus.

Embryo Immunostaining and Mammalian Cell Fixation—Embryos were fixed by the freeze-cracking method in liquid nitrogen, followed by methanol/acetone fixation and rehydration in a descending acetone series modified from Takeda *et al.* (39). P granules were stained by monoclonal K76 antibody (1:5 dilution) (40), followed by FITC-conjugated anti-mouse IgG (1:200, Jackson ImmunoResearch, West Grove, PA). Slides were mounted using VECTASHIELD mounting medium with DAPI (Vector Laboratories, Burlingame, CA). Trans-

fected HEK293T cells were fixed by 4% paraformaldehyde, washed and briefly stained with DAPI. Slides were mounted using VECTASHIELD HardSet mounting medium.

Fluorescence Microscopy—Live and fixed embryo fluorescence imaging and time-lapse microscopy were carried out using a Leica DM RA2 microscope equipped with a Hamamatsu C9100–12 EM-CCD camera. Fixed mammalian cell images were acquired with a Zeiss Axio Imager M2 system. Images were processed in Volocity (PerkinElmer, Waltham, MA) and ImageJ software (41).

Experimental Design and Statistical Rationale—

Quantitative Affinity Purification Assays—Embryos (~2 million per replicate) were freshly harvested in biological triplicate by bleaching young gravid hermaphrodites and sonicated on ice (cycle: 0.5 s, amplitude: 40–45%, 5 strokes/session, 5 sessions, interval between sessions: 30 s; UP200S ultrasonic processor (Hielscher Ultrasonics GmbH)) in lysis buffer (total volume: ~600 μl; 50 mM Tris-HCl, pH 7.4, 100 mM KCl, 1 mM $MgCl_2$, 1 mM EGTA, 1 mM DTT, 10% glycerol, protease inhibitor mixture (Roche), 0.1% Nonidet P-40 Substitute (Sigma)). After sonication, Nonidet P-40 Substitute was added up to 1% and the lysates were incubated with head over tail rotation at 4 °C for 30 min, followed by centrifugation at 20,000 × *g* for 20 min at 4 °C. Cleared lysate was then aspirated without disturbing the upper lipid layer and split by half into either the anti-GFP agarose beads or the blocked control beads (40–50 μl, Chromotek) (Fig. 1*A*). After head over tail rotation at 4 °C for 60–90 min, the beads were washed once with lysis buffer containing 0.1% Nonidet P-40 Substitute, followed by two times of washing in either buffer I (25 mM Tris-HCl, pH 7.4, 300 mM NaCl, 1 mM $MgCl_2$) or buffer II (1 mM Tris-HCl, pH 7.4, 150 mM NaCl, 1 mM $MgCl_2$) or both. For GFP::MBK-2 pull-downs, two separate experiments were performed using different washing conditions. Proteins were eluted by orbital shaking in 50 μl of 6 M urea/2 M thiourea at room temperature. For the MBK-1::GFP pull-down experiments, proteins were eluted twice by shaking in 50 μl of 8 M guanidinium chloride at 90 °C, followed by ethanol precipitation. Eluted protein samples were then digested in-solution as previously reported (19).

For checking the impact of post-lysis interactions, SILAC-labeled "light" BS1080 (GLD-1::GFP) young adults were mixed with "heavy" N2 worms, either before lysis or only at the last washing step before elution (Fig. 2*A*). For the samples mixed before the pull-down, lysates were incubated with anti-GFP agarose beads for 60 min and the bound proteins were eluted in 6 M urea/2 M thiourea. For the samples mixed after the pull-down, the incubation time was 30 min and the elution was performed in 100 mM glycine-HCl, pH 2.5.

For the label-swap SILAC pull-down experiments using HEK293T cells, the EGFP::GEI-12 expressing cells and the control EGFP-only expressing cells were lysed separately in lysis buffer (25 mM Tris-HCl, pH 7.4, 125 mM KCl, 1 mM $MgCl_2$, 1 mM EGTA, 1 mM DTT, 5% glycerol, protease inhibitor mixture, 1% Triton X-100). Cleared lysates were incubated with anti-GFP agarose beads at 4 °C for 90 min, followed by three sequential washes in the following buffers: I (25 mM Tris-HCl, pH 7.4, 125 mM KCl, 1 mM $MgCl_2$, 1 mM EGTA, 0.1% Triton X-100), II (25 mM Tris-HCl, pH 7.4, 125 mM KCl, 1 mM $MgCl_2$, 1 mM EGTA), III (1 mM Tris-HCl, pH 7.4, 150 mM KCl, 1 mM $MgCl_2$). Beads of the two SILAC states were combined before the final wash. Proteins were eluted using 8 M guanidinium chloride, ethanol precipitated and further processed as mentioned above. To check whether GEI-12 interactions were partially mediated by RNA, pull-down experiments against EGFP::GEI-12 were performed using cell lysates pre-treated with or without nuclease (250 U, Pierce Universal Nuclease, Thermo Scientific) for 20 min.

Pull-down Simulation Experiment—To simulate the detection of label-free pull-down enrichment in a complex nonspecific background, two samples of predefined composition were prepared: sample 1: 1× *E. coli* lysate, 1× UPS2 human standard (Sigma Aldrich), recombinant CDC42 (gift from Florian Paul); sample 2: 1× *E. coli* lysate, 4× UPS2 human standard, recombinant RAC1, RHOA, and GFP. These two samples were measured in succession in triplicate.

Liquid Chromatography Tandem Mass Spectrometry—Peptide mixtures were separated by reversed phase chromatography using the Eksigent NanoLC Ultra system or the EASY-nLC system (Thermo Scientific) on a 20-cm fritless silica microcolumn (inner diameter: 75 μm) packed in-house using ReproSil-Pur C18-AQ 3-μm resin (Dr. Maisch GmbH). Peptides were separated on an 8–50% acetonitrile gradient (120 min or 200 min) with 0.1% formic acid at a nanoflow rate of 200 nl/min. Eluting peptides were directly ionized by electrospray ionization and transferred into an LTQ Orbitrap Velos or a Q Exactive Quadrupole-Orbitrap mass spectrometer (Thermo Scientific). Mass spectrometry was conducted using data-dependent mode with one full scan followed by fragmentation scans of the ten most intense ions using a sensitive method.

Mass Spectrometry Data Analysis—Raw data files were processed with default settings (unless stated otherwise) in MaxQuant version 1.4.1.2 (42) using the built-in Andromeda search engine (43) against a target-decoy database containing the forward and reverse sequences: for embryo pull-downs, WormPep release WS245 (27,368 entries) and *E. coli* K-12 MG1655 proteome (4285 entries); for HEK293T cells, Uniprot human proteome release 201402 (88,665 entries). Common contaminants (247 entries), such as Keratins, were also included in the database search. Trypsin/P specificity was used for all data except for SILAC worm data for which LysC/P specificity was applied. Carbamidomethylation of cysteine was used as fixed modification; oxidation of methionine and acetylation of the protein N terminus were set as variable modifications. Minimal peptide length of 7 amino acids was required and a maximum of two missed cleavages were allowed. The "second peptide" option was chosen to decipher co-fragmented MS/MS spectra. False discovery rate was set to 1% for both peptide and protein identifications. Each protein group was required to contain at least one unique peptide. Only the first member of each protein group was considered for further analysis.

For embryo label-free pull-down experiments, protein quantification was performed using the label-free quantification (LFQ) algorithm (44). Minimum LFQ ratio count was set to one. Both unique and razor peptides were considered for quantification. Retention times were recalibrated using the default nonlinear time-rescaling algorithm. The "match between runs" option was chosen for transferring MS/MS identifications between LC-MS/MS runs with the maximal retention time window set to 1 min. Only proteins quantified in at least two out of the three GFP pull-down replicates were included in the analysis. LFQ intensities were $\log_2$-transformed and imputation for missing values was performed in Perseus software (version 1.2.0.17) based on a simulated normal distribution to represent low abundance values below the noise level (width = 0.3; shift = 1.8). The LFQ abundance ratio was then calculated for each protein between the GFP pull-downs and the controls. Significance of the enrichment was measured by two-sample Student's *t* test assuming equal variances. Specific interaction partners were then determined in a volcano plot where a combined threshold (hyperbolic curve) was set based on a modified *t*-statistic (*t*(SAM, statistical analysis of microarrays); s_0 = 1.5, t_0 = 0.9 ~ 1.1) (45, 46). Threshold values were chosen to balance sensitivity and false discovery rate based on the simulation experiment with spike-in standards (supplemental Fig. S2). Proteins cross-reactive to the anti-GFP beads were identified by a pull-down assay using N2 embryos (supplemental Fig. S1). These proteins as well as HDA-3, a protein identified in almost all other pull-downs, have been filtered out from the IVI data. Raw data files have been deposited on PRIDE proteomics data repository (accession no. PXD002624).

For SILAC pull-down experiments in mammalian cells, maximum of 3 labeled amino acids per peptide were allowed. "Requantify" option was chosen. Only proteins quantified in both forward and reverse experiments were considered for analysis with a minimum SILAC ratio count set to one.

SDS-PAGE and Western Blotting—Proteins were resolved in a NuPAGE 4–12% gradient gel (Invitrogen) and transferred to a PVDF membrane. Blocking was done in 5% nonfat milk in TBST buffer (25 mM Tris-HCl pH 7.4, 150 mM NaCl, 0.05% (v/v) Tween-20) for 1 h, followed by primary antibody incubation at 4 °C overnight. Primary antibody dilutions were: 1:500 anti-CAR-1 (47), 1:500 anti-IFET-1 (48), 1:250 anti-SPN-4 (49), and 1:2,000 anti-γ-Tubulin (Sigma-Aldrich). The membrane was then incubated with horseradish peroxidase-conjugated secondary antibodies (1:10,000) at room temperature for 1 h, followed by brief incubation with substrates for enhanced chemiluminescence (Pierce ECL Plus, Thermo Scientific, Waltham, MA). Signal was detected by a GE Typhoon FLA 9000 biomolecular imager at 473 nm excitation wave-length with an LPB filter.

Statistical and Network Analyses—Statistical and network analyses were performed using R, Bioconductor and Cytoscape. GO enrichment analysis for CAR-1 PPIs was conducted using the GOstats package (50). Other enrichment analyses were done based on the hypergeometric distribution. RNAi and GO annotations were retrieved from WormBase release WS245. For comparison analysis with IVI, homomeric interactions and interaction pairs containing "dead" genes, which are no longer valid gene model entries in WS245, were removed from the WI8 and LCI data sets. The WI8 embryo lethal subset was based on WI8 interactions in which at least one protein of each interacting pair is annotated with the "embryonic lethal" RNAi phenotype. Different alternative splicing isoforms of the same gene were collapsed into one. Interaction partners identified in two separate GFP::MBK-2 pull-down experiments were combined. Known interactions in IVI network were retrieved from GeneMANIA database (version: 1 June 2014; physical interactions only) and STRING database (version 10; experimental data only; evidence threshold: 0.40). For enrichment analyses, control gene sets were generated by selecting 3000 pairs of protein-coding genes at random from WormPep (WS245). The mean percentage of gene pairs with shared RNAi phenotypes or GO terms across 100 iterations of independent control sets was then used for comparison with the IVI, WI8, and LCI interactome data sets.

RESULTS

Quantitative Proteomics Detects Protein-Protein Interactions in Worm Embryos—We reasoned that combining quantitative proteomics and the widely available GFP-fusion strains should allow us to explore PPIs in *C. elegans* embryos (Fig. 1 *A*). We first established the procedure using specific test cases before using it to develop our initial PPI map. Our general strategy involved collecting early *C. elegans* embryos that express GFP-fusion proteins from gravid hermaphrodites, followed by pulling down the GFP-fusion protein (together with its interaction partners) using anti-GFP antibodies coupled to agarose beads.

The principle of quantitative affinity purification and mass spectrometry (q-AP-MS) is to compare the abundance of proteins in a pull-down with a negative control (19–21). There are two possibilities for negative controls: First, control pull-downs can be performed with anti-GFP antibodies on worm samples that do not express the GFP-fusion protein of interest. Second, control pull-downs can be carried out with the same worm samples that express the GFP-fusion protein but using control beads lacking conjugated antibodies. The advantage of the second option is that the same input is used for the experiment and the control pull-down. Therefore, results are not affected by factors such as differences in protein abundance between strains and variability in lysate preparation. We therefore followed this strategy and incubated the same embryo lysate with control beads lacking conjugated antibodies. The proteins in both pull-downs were then identified by high resolution shotgun proteomics. In order to distinguish specific interaction partners from nonspecific contaminants, we compared the abundance of proteins in both pull-downs using label-free quantification. Proteins were considered specific interaction partners of the bait protein when they were significantly more abundant in the anti-GFP pull-downs than in controls.

Because worm proteins that were cross-reactive to the antibody would also be enriched in the anti-GFP pull-downs, we therefore performed additional control experiments using the same strategy with wild-type N2 worm embryos that do not express GFP-fusion proteins. These control experiments revealed that the background binding profiles of anti-GFP beads and control beads are very similar (supplemental Fig. S1). Cross-reactive proteins that showed significant binding to anti-GFP beads in these N2 experiments were removed from the final sets of interaction partners for all GFP fusion proteins.

To test the label-free quantification accuracy of our technical setup, we conducted a benchmark experiment to simulate the detection of enriched interactions in a complex nonspecific binding background (supplemental Fig. S2). We analyzed two samples with defined protein composition that each contained the same amount of *E. coli* whole cell lysate (to simulate background binders). In addition, the samples contained a mixture of 48 different isolated or recombinant human proteins (UPS2 standard) in a 1:4 ratio. Finally, four additional recombinant proteins were exclusively spiked into one of the two samples. We found that our method correctly identified 29 out of 32 detected differential binders. Conversely, 1174 out of 1184 background binders were correctly classified as such. In total, the accuracy was 98.9% and the precision 90.6%. This experiment demonstrates the high accuracy and precision of our label-free interaction proteomics approach.

To test our approach in *C. elegans* embryos, we targeted the RNA-binding protein CAR-1, whose interaction with the RNA helicase CGH-1 is evolutionarily conserved (47, 51, 52). We pulled down GFP::CAR-1 from about 2 million transgenic embryos in three biological replicates. We then assessed the abundance of proteins identified in the GFP::CAR-1 pull-downs and three control experiments performed in parallel. We used the Student's *t* test to assess which proteins were significantly more abundant in the GFP::CAR-1 pull-downs than in the controls. The data can be visualized in a volcano plot that displays both the enrichment ratio and the signifi-

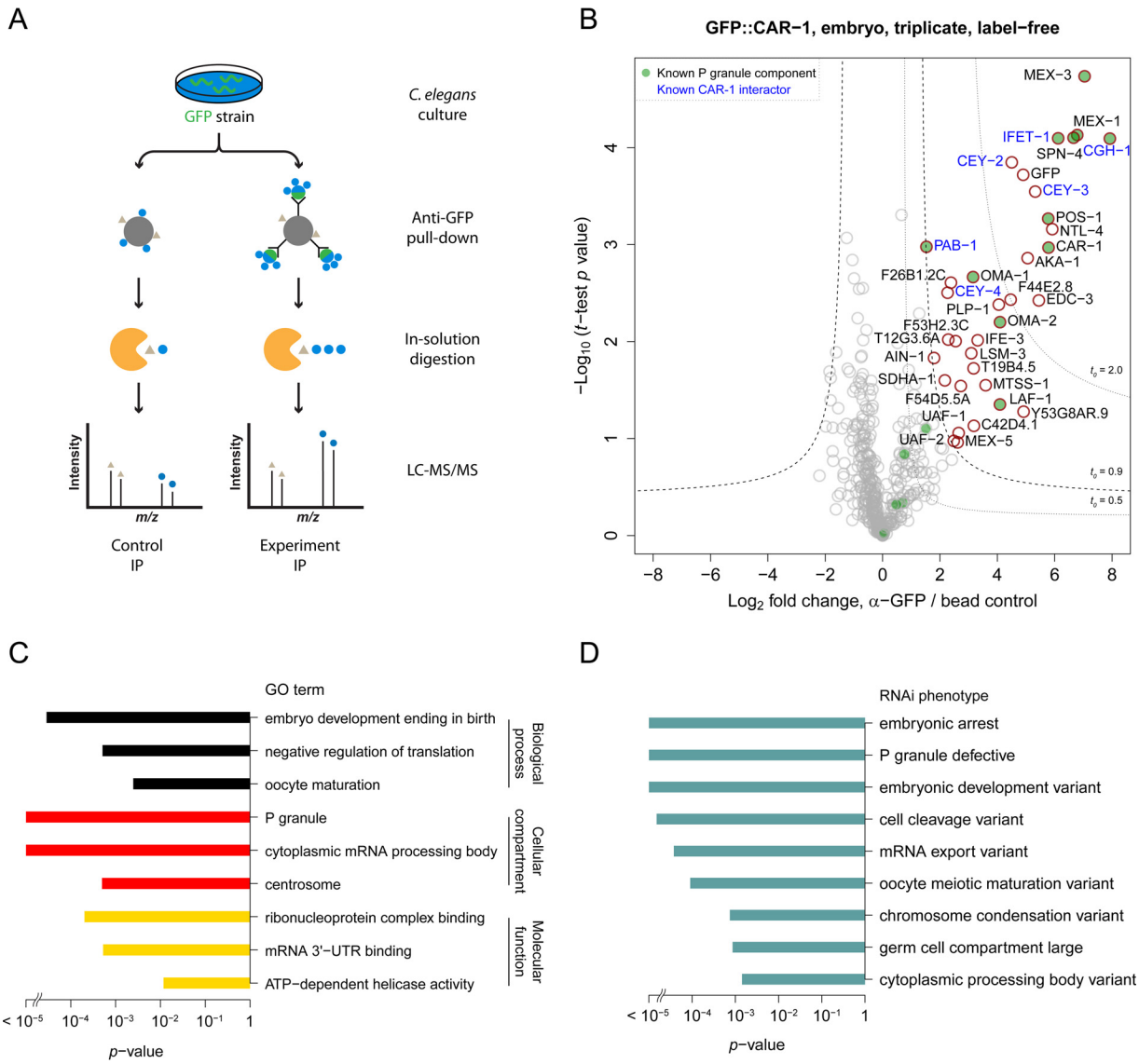

FIG. 1. **Label-free embryo interaction proteomic strategy and proof-of-concept experiment.** *A*, Experimental design. Samples of the same extract from worm embryos expressing GFP-protein fusions were incubated separately with anti-GFP conjugated or control beads, and abundances of co-purified proteins were measured by mass spectrometry. *B*, Volcano plot showing specific interaction partners of GFP::CAR-1 based on pull-down experiments of biological triplicate. Interaction partners meeting stringency thresholds (hyperbolic curves, $t_o = 0.9$) are shown in red. To exemplify the effect of various stringencies, two extra curves of high cut-off ($t_o = 2.0$) and low cut-off ($t_o = 0.5$) are drawn. Known CAR-1 interactors are colored in blue. Known P granule components detected in the pull-downs are shown in green. *C*, GO term enrichment analysis for the interaction partners of GFP::CAR-1. Selected significantly enriched GO terms are displayed (conditional hypergeometric test). *D*, RNAi phenotype enrichment analysis for the interaction partners of GFP::CAR-1. Selected significantly enriched RNAi phenotypes are shown (hypergeometric test).

cance (Fig. 1*B*). Specific interaction partners were then selected using a combined cut-off that takes both the significance and the enrichment ratio into account (22, 45, 46). We determined the cut-off values to balance sensitivity and false discovery rate based on the simulation experiment described above. As expected, most of the 429 identified proteins had either low enrichment ratios or high *p* values, indicating that they are nonspecific contaminants. In total, 34 proteins were significantly enriched in the GFP::CAR-1 pull-downs compared with controls and were thus considered specific interaction partners. With the exception of ATX-2 and PATR-1, this set of proteins contains all proteins known to interact with both CAR-1 and CGH-1 *in vivo* (CEY-2, CEY-3, CEY-4, IFET-1, PAB-1) (47, 48, 51). Thus, our strategy can capture *in vivo* interactions with good sensitivity. We also observed enrichment of Gene Ontology (GO) terms like “P granule” and “oocyte maturation” in the interactome (Fig. 1*C*). This is consistent with the known association of CAR-1 with P granules and its role in oocyte development (47, 53). Interestingly, we also observed enrichment of centrosomal proteins, which

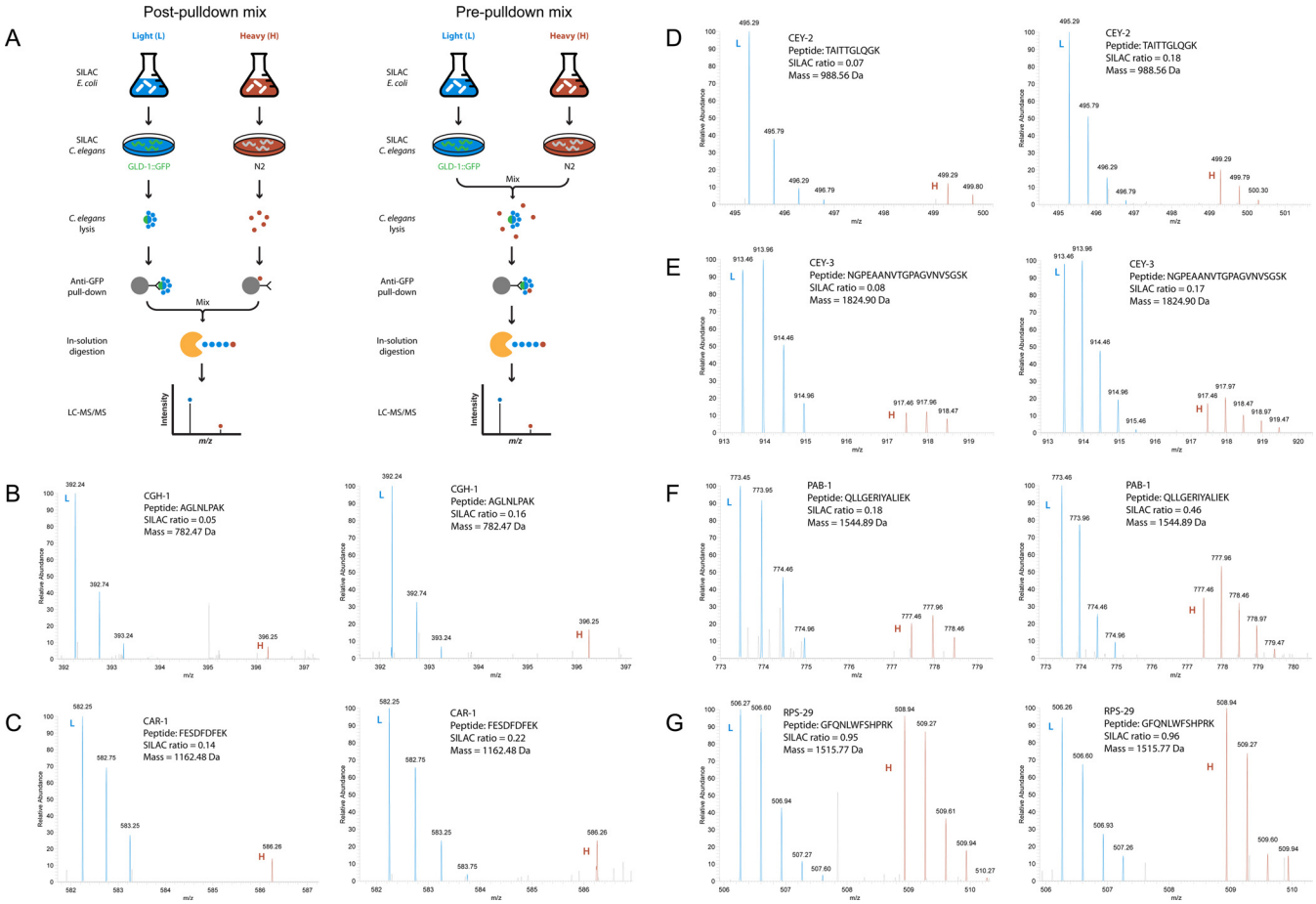

FIG. 2. **Interaction proteomics detects mainly interactions formed *in vivo*.** *A*, Experimental designs using *in vivo* SILAC. Worms harboring GFP fusion proteins were fed on bacteria with light label (L); control N2 worms were fed on bacteria with heavy label (H). Worm lysates were combined either prior to affinity purification with anti-GFP beads, or after independent pull-downs with anti-GFP and control beads, then the combined samples were subjected to mass spectrometry. *B–F*, Representative mass spectra showing peptides of several known interaction partners of GLD-1 (CGH-1, CAR-1, CEY-2, CEY-3, PAB-1). Preferential recovery of the light form in both treatments indicated that minimum binding occurred post-lysis; *G*, the nonspecific binder, RPS-29, was identified equally in light and heavy forms. A relative increase in the heavy form of PAB-1 when lysates were mixed prior to pulldowns suggested that PAB-1 is in dynamic exchange with a pool of free PAB-1 and/or also binds to GLD-1 *in vitro*. Light peptides are shown in blue; heavy peptides are shown in red.

may be of particular relevance to the phenotypic defects in anaphase spindle structure and cytokinesis that are associated with depletion of CAR-1 in *C. elegans* embryos (52). Similarly, when we compared known RNAi phenotypes of CAR-1 interaction partners, we found the phenotypes "P granule defective", "oocyte meiotic maturation variant," and "cytoplasmic processing body variant" to be enriched (Fig. 1*D*). We also confirmed our identification of SPN-4 as a novel CAR-1 interaction partner on Western blots using antibodies against SPN-4 (supplemental Fig. S3). Collectively, these data indicate that our interactome captures important aspects of known CAR-1 biology.

The CAR-1 experiments showed that the sensitivity of the approach can be high. However, the specificity is more challenging to determine. In addition to using stringent cut-off values and comparing to control pull-downs, a particularly vexing source of possible false positives might arise from interactions that would form postlysis. This means that a bait protein could theoretically be co-purified with proteins expressed in different tissues. We investigated this possibility using the test case of GLD-1, a protein that is expressed only in the germline (54). To assess the potential impact of post-lysis interactions on our results, we mixed young adult worms expressing GLD-1::GFP with wild-type N2 worms that were metabolically labeled with heavy stable isotopes using SILAC, as previously described (27). We reasoned that with this experimental design (Fig. 2*A*), *in vivo* interaction partners should be present in the light form, whereas post-lysis (*i.e. in vitro*) interactions should lead to a heavy-to-light ratio of 1:1. Our mass spectrometry data showed that peptides derived from known GLD-1 interaction partners (55) were predominantly detected in the light form (Fig. 2*B–2F*). This is particularly remarkable given that whole worms were used for this experiment, whereas GLD-1 is only expressed in the germline.

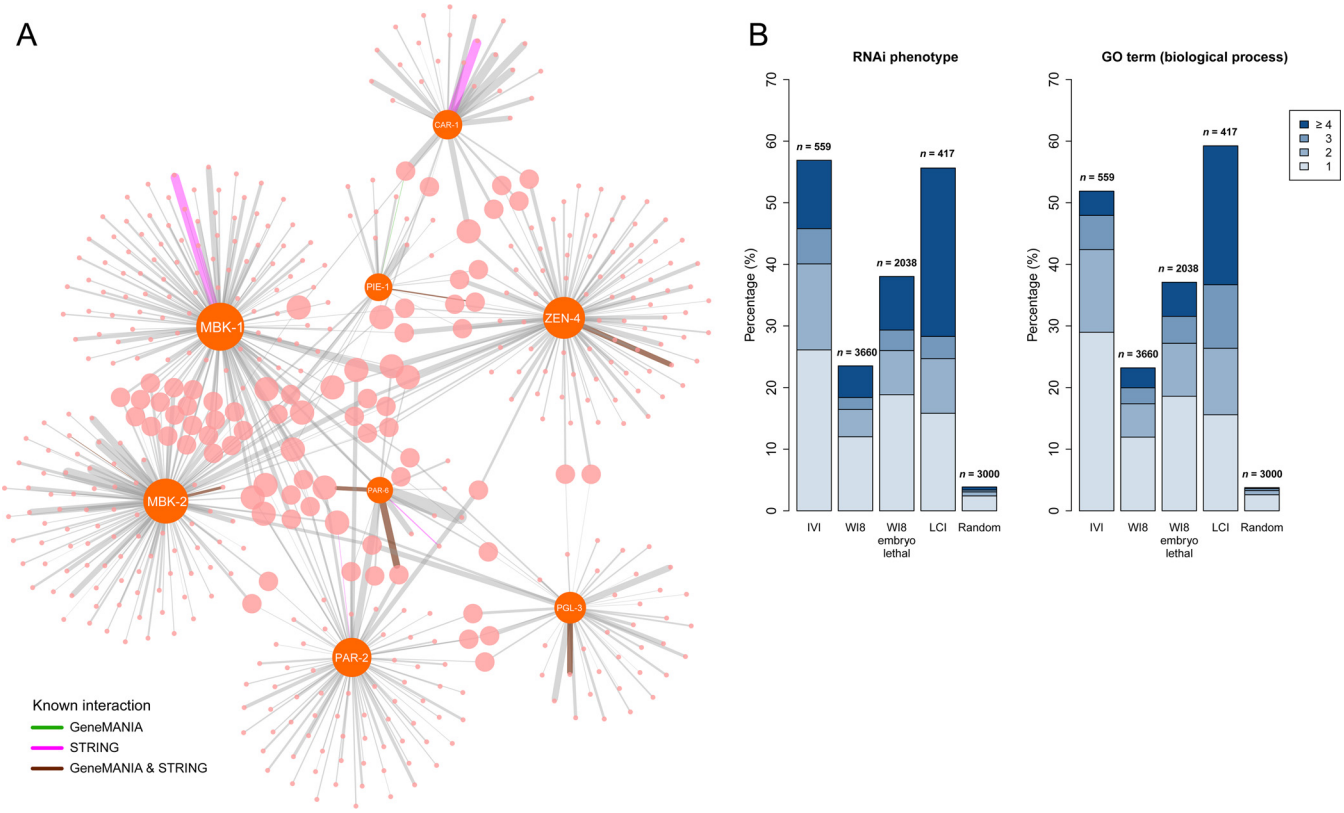

FIG. 3. **Embryo *in vivo* interactome (IVI) map and enrichment of shared functions for IVI partners.** *A*, Embryo IVI map. Bait (orange) and prey (pink) proteins are shown as nodes sized proportionally to their degree distribution. Edges for known interactions are colored according to STRING database (green), GeneMANIA database (magenta) or both (brown). Thickness of the edges is weighted based on the *t* (SAM) statistic (See supplemental Fig. S4 for high-resolution network diagram.) *B*, Stacked bar charts showing the percentages of interacting protein pairs that share at least one annotated RNAi phenotype or Biological Process GO term for IVI, WI8, WI8 subset (at least one protein of each interacting pair is annotated with the "embryonic lethal" RNAi phenotype) and LCI *versus* random sets of gene pairs (percentages are mean values based on 100 random samples of size 3,000 from all protein-coding genes).

Thus, our pull-down conditions appear to mainly identify known GLD-1 interactions from pre-existing complexes that are formed before lysis.

A Pilot Protein-Protein Interaction Network for C. elegans Embryogenesis—Having shown that we can identify *in vivo* PPIs in worm embryos, we next extended our strategy to a set of proteins that were selected according to the following characteristics. First, we sought established *C. elegans* lines expressing GFP fusion proteins that are either capable of rescuing loss of the endogenous gene and/or show a localization pattern mirroring that of the endogenous protein in the early embryo. Second, because we wanted to understand how proteomics using embryos could facilitate the study of essential developmental processes, we selected proteins with essential functions in the *C. elegans* early embryo. Finally, within the broad scope of early embryonic development, we wanted to explore more than one biological process. We thus included proteins involved in polarity establishment and development (MBK-2, PAR-2, PAR-6, ZEN-4) and P granule assembly/regulation (CAR-1, PGL-3, PIE-1). In addition, we also included MBK-1 which is a nonessential paralog of MBK-2 and is known to be involved in neuronal development (29) but not in embryonic polarity. Quantitative *in vivo* interaction proteomics for all bait proteins generated a combined network of 559 interactions between 472 proteins (Fig. 3*A*; see supplemental Fig. S4 and supplemental Table S1 for a complete list with all IDs). Considering that we only performed pull-downs for eight bait proteins the number of detected interactions is remarkable. Our map contains several interactions known to be relevant during embryogenesis, such as the evolutionarily conserved PAR-3/PAR-6/PKC-3 complex (10), the binding of PAR-6 and LGL-1 (56), the interaction of PAR-2 and PAR-1 (11), the centralspindlin motor complex of ZEN-4 and CYK-4 (57), and the association of PGL-3/SEPA-1/EPG-2, which mediates the autophagic degradation of P granules in somatic blastomeres (58, 59). However, most of the interactions we identified are novel.

The main value of PPI data is that it provides mechanistic insights into biological processes. For example, because interacting proteins are often involved in the same biological pathway, inactivating the corresponding genes frequently results in the same phenotype (60, 61). In *C. elegans,* RNAi

phenotypes provide a valuable resource to assess the functional relationship between genes *in vivo*. To test the functional relevance of our *in vivo* interactome (IVI) data, we therefore analyzed the proportion of interacting proteins that share RNAi phenotypes. Intriguingly, we found that more than 50% of all PPIs in IVI have at least one RNAi phenotype that is shared between both proteins (Fig. 3*B*). This fraction is about 10 times higher than expected for random protein pairs ($< 5\%$ in 100 control sets). For comparison, we repeated this analysis for yeast two-hybrid-based data (worm interactome version 8, WI8) and literature curated interactions (LCI) (6). We found that the fraction of PPIs with shared RNAi phenotypes in IVI is on par with LCI and considerably higher than in WI8. Our bait proteins were selected based on their essential function in early embryogenesis. To compensate for this selection bias, we also restricted the WI8 data set to interactions where at least one protein of each pair is annotated with the "embryonic lethal" RNAi phenotype. We found that IVI still outperforms this "WI8 embryonic lethal" subnetwork. Similar results were obtained for shared GO terms (Fig. 3*B*). In summary, these analyses strongly support the high biological relevance of our *in vivo* interactome data.

Identification of the MBK-2 Binding Partner GEI-12 as a Novel Protein Required for P Granule Assembly—Having shown that our *in vivo* interaction map contains functionally relevant information, we next asked if these data would allow us to better understand embryonic development. To this end, we focused on P granule assembly. Like other types of RNP granules, P granules are microscopically visible assemblies of RNAs and proteins (62). Mutations in genes encoding P granule components often cause sterility, indicating that they are key determinants of germ cell identity (12). In the one-cell embryo, P granules are initially distributed evenly throughout the cytosol. Before the first cell division, they localize to the posterior half of the zygote and subsequently segregate with the P lineage. Microscopic studies have shown that P granules are highly dynamic and show liquid-like behavior (13). However, the molecular signaling mechanisms that regulate assembly and disassembly of RNP granules (including P granules) have not been completely elucidated.

MBK-2, a member of the dual-specificity tyrosine-regulated kinase (DYRK) family, is an important regulator of the oocyte-to-embryo transition (reviewed in 63) that also influences P granule assembly (30, 64). We confirmed this finding by performing time lapse microscopy in GFP::PGL-3 embryos (supplemental Movie S1 and S2): while control RNAi embryos showed the expected segregation of P granules to the P lineage, *mbk-2(RNAi)* animals displayed ectopic granules in somatic blastomeres. We asked if our PPI data for MBK-2 could help us to characterize its role in P granule assembly *in vivo*. Before fertilization, MBK-2 is sequestered at the oocyte cortex via interaction with the cortical anchors EGG-3 and the pseudo-phosphatases EGG-4/5 (65–67). Consistently, we detected binding of MBK-2 with EGG-3/4 and CHS-1, a protein involved in egg shell synthesis (68). Interestingly, we also detected as MBK-2 interaction partners several known P granule components, *i.e.* CCF-1, GLD-2/3, DRH-3, and MEG-2.

Because most of the interaction partners we identified for MBK-2 had no known role in P granule assembly, we investigated whether any of them also showed a P granule phenotype in embryos, using RNAi knock-downs with GFP::PGL-1 and GFP::PGL-3 as P granule markers. Of 40 genes tested, depletion of only one - *gei-12* - displayed a discernible P granule phenotype (Fig. 4). In embryos, knocking down *gei-12* disrupted the localization of both PGL-1 and PGL-3 to P granules: while control embryos showed proper segregation of these markers to the P lineage, *gei-12(RNAi)* embryos displayed diffuse GFP signal throughout all cells and lacked detectable granule formation in the germline progenitor. These results were also confirmed by antibody staining against endogenous P granule proteins (supplemental Fig. S5).

P granule assembly has previously been shown to involve a hierarchy of genetic components (12). We investigated the role of *gei-12* in this hierarchy and found that recruitment of GLH-1, a protein that acts upstream of PGL-1 and PGL-3 in P granule assembly (12, 69), was also impaired by RNAi of *gei-12* (Fig. 4). Thus, *gei-12* acts upstream of *pgl-1/3* and *glh-1* in the hierarchy of P granule assembly in the early embryo. We also found that *gei-12* is required for the enrichment of MBK-2 in the P lineage (Fig. 4). However, several other posteriorly localized components such as CAR-1, PIE-1, POS-1 and SPN-4 still segregated properly when *gei-12* was depleted (supplemental Fig. S6). Therefore, *gei-12* is needed to recruit a distinct subset of P granule components, including PGL-1/3, GLH-1 and MBK-2, but is dispensable for the asymmetric localization of other proteins. Finally, our results indicate that *gei-12* is specifically required for P granule assembly in the embryo, because its depletion did not detectably disrupt the formation or localization of P granules in the parental germline of adult RNAi-treated worms (Fig. 4). Next, to investigate the localization of GEI-12 in embryos, we created a transgenic GEI-12::GFP line. We observed a perinuclear pattern in the developing germline and granular structures in the cytoplasm of maturing oocytes (Fig. 5*A*). In embryos, GEI-12::GFP localized to the posterior at the one-cell stage and segregated with the P lineage as embryonic cell division progressed. Thus, the distribution of GEI-12 resembles that of P granules in early development.

GEI-12 has two known paralogs, C36C9.1 and F52D2.12. To further characterize the function of these paralogs, we performed additional experiments to investigate their potential roles and functional redundancy in P granule assembly. When we stained P granules using antibodies in available lines harboring mutations in these genes, we found that neither of two *gei-12* deletion mutant strains (*tm4526* and *tm4259*) showed a P granule phenotype, nor did the C36C9.1

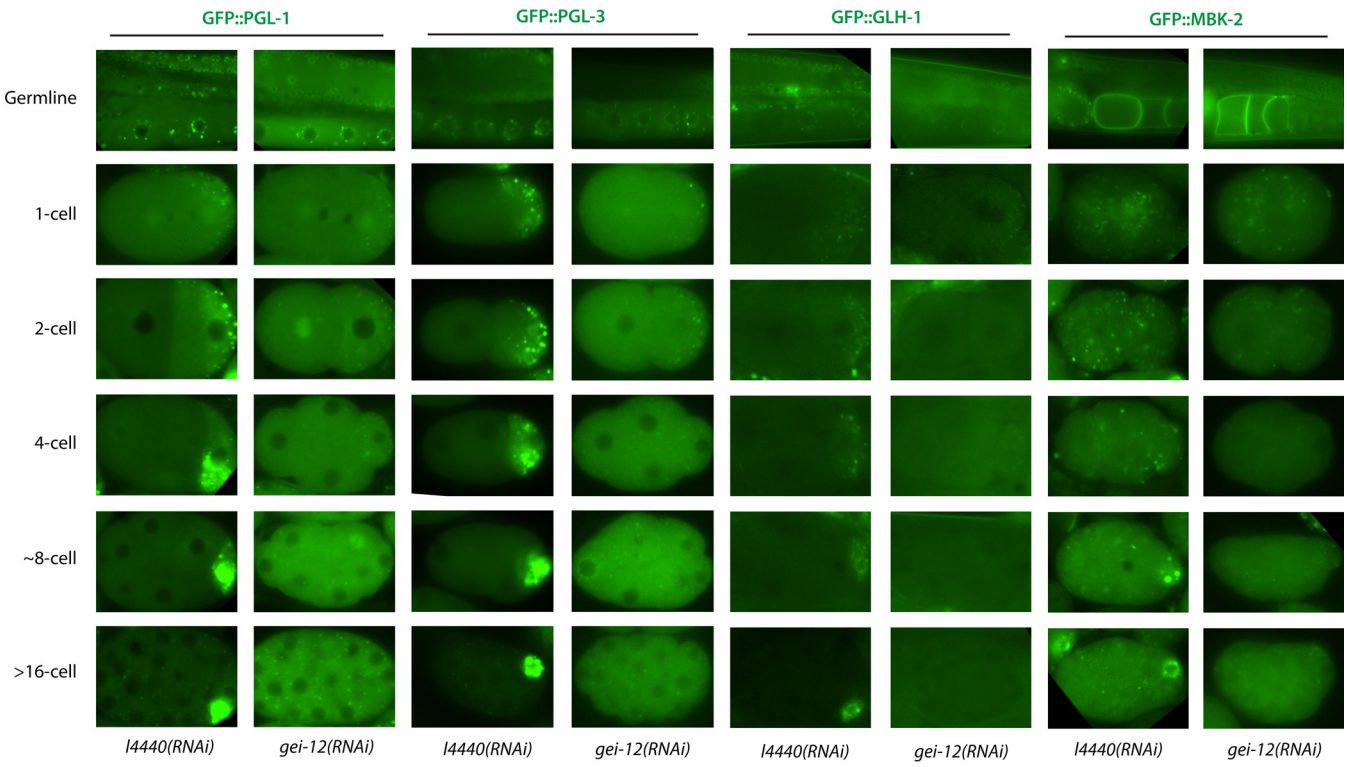

FIG. 4. **GEI-12 is a novel protein required for P granule assembly.** Depletion of *gei-12* by RNAi affected P granule assembly specifically during early embryogenesis but not prior to fertilization, as visualized in live embryos harboring GFP fusions of several proteins that localize to P granules. *L4440(RNAi)* served as control.

mutant strain (*tm4343*) (supplemental Fig. S7). Knocking down C36C9.1 and F52D2.12 individually by RNAi in wild-type animals also did not impair P granule assembly (supplemental Fig. S5). Combined with our *gei-12(RNAi)* results, which did show a P granule phenotype, it appears that the paralogs of *gei-12* are efficiently targeted by the *gei-12* RNAi clone, and that there is some functional redundancy among them. Indeed, the *gei-12* RNAi clone shows a high degree of sequence similarity with C36C9.1 and F52D2.12. When we tested the functional significance of this, we found that knocking down C36C9.1 in either *gei-12* mutant strain disrupted P granule assembly with higher penetrance than in wild-type worms (supplemental Fig. S7). From these experiments, we conclude that *gei-12* and its paralogs are critically involved in P granule assembly in a partially redundant manner.

GEI-12 is Required for Germline Maintenance—Compromising multiple P granule components simultaneously has been reported to produce sterility after more than one generation of RNAi (70). In a similar fashion, L1 larvae treated with *gei-12* RNAi initially remained fertile upon reaching adulthood; however, continuous application of *gei-12* RNAi to the progeny by feeding resulted in sterility in about 5% of the F1 generation and up to 30% of the F2 generation at 15 °C, and these percentages increased up to 35 and 68% when the test was performed at 25 °C (Fig. 6*A*). Sterile worms had empty uteri and extremely reduced germlines with no gametes, both in hermaphrodites and in males (Fig. 6*B*–6*C*). We conclude that *gei-12* is an important maternally provided germline factor that is required in the embryo for fertility and germline proliferation, and that this requirement increases with temperature. Similar findings were previously reported for the P-granule components *meg-1* and *meg-2* (71).

GEI-12 Forms Granules in Mammalian Cells—GEI-12 does not have clear orthologs outside nematodes, nor does it have predicted protein domains. The protein is remarkably rich in serine and threonine residues (~20%) and contains several predicted low complexity (LC) regions (Fig. 5*B*). Recently, LC regions have been reported to be both necessary and sufficient for RNP granule formation in a cell free system (72). We therefore wondered if GEI-12 can itself induce granules in the absence of other *C. elegans* factors. To test this possibility, we expressed EGFP::GEI-12 in HEK293T cells. Indeed, we observed the formation of multiple fluorescent granules (Fig. 7*A*). Thus, GEI-12 can drive granule formation in mammalian cells, similar to previous observations for PGL-1/3 (73). To further characterize these GEI-12-positive granules in HEK293T cells, we used SILAC-based quantitative interaction proteomics to identify specific interaction partners (19, 20). We found that EGFP::GEI-12 specifically interacted with nearly 300 mammalian proteins (Fig. 7*B*). Most of these proteins are well-known RNA binding proteins such as FXR-1/2,

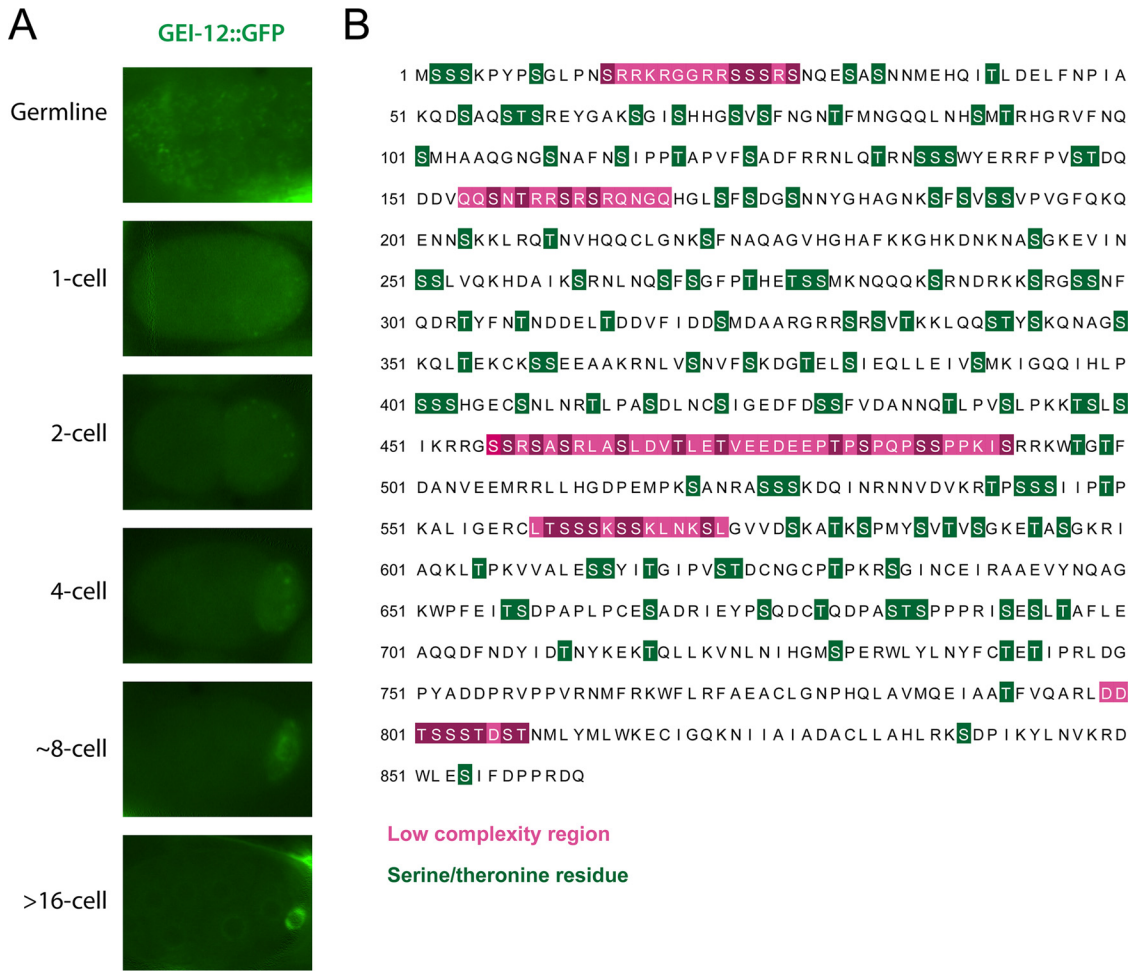

FIG. 5. **GEI-12 forms granules *in vivo* and segregates exclusively with the P lineage.** *A*, Transiently expressed GEI-12::GFP formed granules in vivo in the adult germline and zygote, and these segregated to the P lineage during early embryogenesis in a localization pattern resembling that of P granules. *B*, The sequence of GEI-12 contains several predicted low complexity regions (highlighted in magenta) and a high proportion of serine/threonine residues (19.4%, highlighted in green). Prediction was performed in SMART database using the SEG algorithm with default parameters (82).

Staufen, translation initiation factors and ribosomal proteins. About 10% of these proteins are known components of different types of RNP granules (72), which represents a highly significant enrichment (p value $= 6 \times 10^{-21}$, hypergeometric test). A notable additional class of proteins were components of the protein phosphatase 2A (PP2A) family (discussed below). Thus, GEI-12 positive granules contain many known mammalian RNP granule components. This is surprising, especially because GEI-12 has no known mammalian ortholog. Combined with the observations that GEI-12 is (1) required for P granule formation in worms, and (2) forms granules in mammalian cells, our results suggest that this protein plays a functionally conserved role in the assembly of RNP granules, and that the primary determinant of this activity resides in physical properties of the protein. Most of the proteins co-purifying with GEI-12 are not affected by nuclease treatment, suggesting that they are not RNA dependent (Fig. 7*C*).

Kinase and Phosphatase Interplay Regulates P Granule Assembly During Early Embryogenesis—The molecular signaling mechanisms that regulate the assembly and disassembly of RNP granules (including P granules) are not entirely understood. *mbk-2(RNAi)* embryos displayed ectopic granules outside the germline ((30), Fig. 8 and supplemental Movie S2). In mammals, dissolution of stress granules is driven by DYRK3, a homolog of MBK-2 (74). Hence, the kinases DYRK3 and MBK-2 might induce granule dissolution by phosphorylating specific substrates. In this context, it is particularly intriguing that we identified several proteins belonging to the PP2A family of phosphatases as GEI-12 interaction partners in mammalian cells (Fig. 7*B*). This set of proteins included the catalytic subunit (PPP2CA), structural subunits (PPP2R1A, PPP2R1B) and, specifically, several regulatory subunit B56 subfamily members (PPP2R5A, PPP2R5C, PPP2R5E). This is significant because, in our MBK-2 pull downs, we also iden-

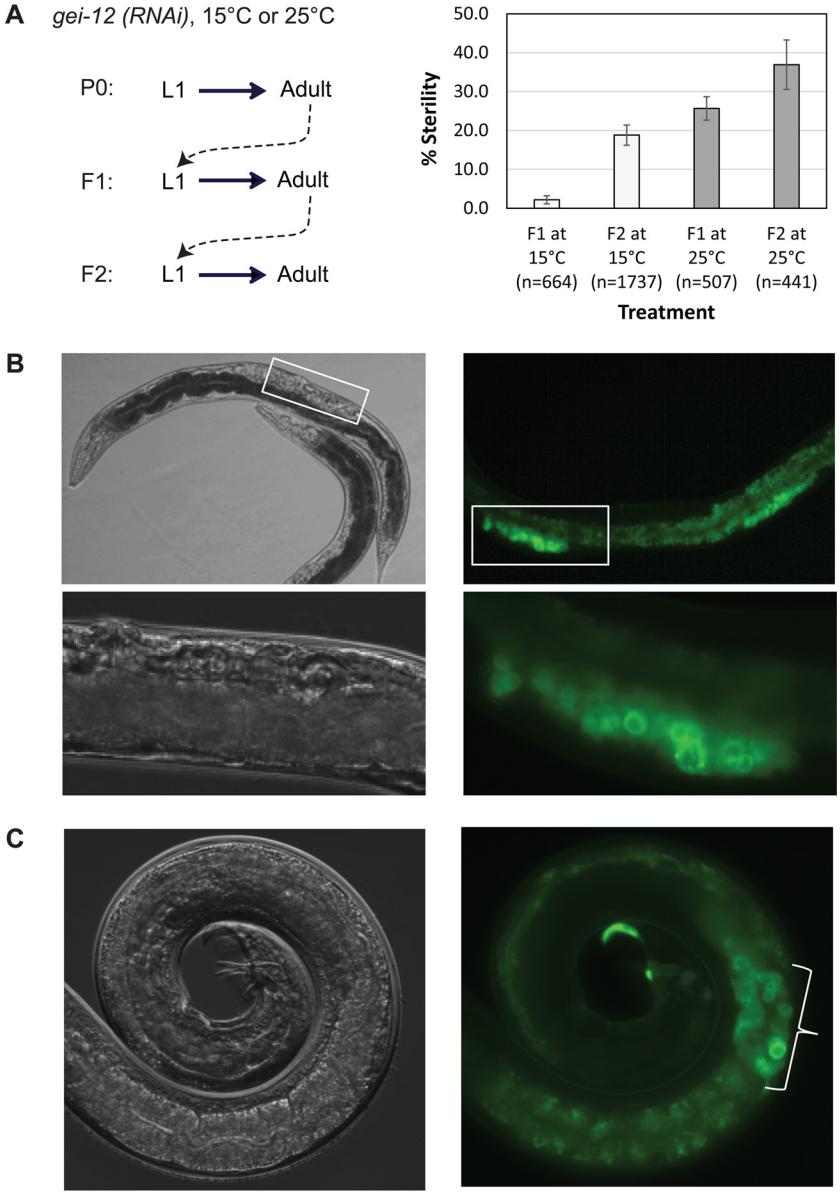

FIG. 6. **GEI-12 is required for germline proliferation and gamete formation.** *A*, Left: Protocol for continuous generational RNAi of gei-12 by feeding. Right: Average sterility rates among adult progeny in first (F1) and second (F2) filial generations, with standard error. Adults from the P0 generation were not sterile; sterility among adult progeny increased with generation and temperature. *B*–C, Examples of adult hermaphrodite (B) and male (C) progeny after generational *gei-12(RNAi)* treatment. Light micrographs (left) and GFP::PGL-1 (right) show reduced germlines with fewer PGL-1 positive cells in both sexes. Sterile hermaphrodites also show empty uteri devoid of embryos. Bottom panels in (B) show magnified view of highlighted boxes in upper panels. In (C), bracket spans region of defective male germline.

tified PPTR-2, a *C. elegans* ortholog of the B56 subfamily (supplemental Fig. S4 and supplemental Table S1). PPTR-2 has also been reported to physically interact with GEI-12 and its paralog C36C9.1 in yeast two-hybrid screens (6). Moreover, another worm ortholog of the B56 subfamily, *pptr-1*, has previously been shown to be required for P granule assembly (75). In fact, the phenotypes of *pptr-1* mutants and *gei-12(RNAi)* worms are strikingly similar. We therefore tested if depleting *mbk-2* could rescue the P granule phenotype of *pptr-1* mutant embryos. As previously described (75), we observed that *pptr-1* mutant embryos showed strongly reduced P granules at the one- and two-cell stages that further diminished during embryonic cell divisions (Fig. 8). Intriguingly, knocking down *mbk-2* by RNAi restored P granule formation in the *pptr-1* mutant (Fig. 8). Hence, *mbk-2* and *pptr-1* appear to mediate P granule dissolution and formation, respectively. Taken together, these findings strongly suggest that GEI-12 may orchestrate the dynamics of P granules by interacting with the kinase MBK-2 and the phosphatase PP2A.

DISCUSSION

Identifying interaction partners in the context of a living animal is arguably the most informative single data set to characterize protein function. Very few studies have reported the systematic isolation of interaction partners in animal tissues for multiple bait proteins (76), and no such studies have, to our knowledge, been performed using isolated *C. elegans* embryos. To the best of our knowledge, our initial network of 559 interactions among 472 proteins represents the first *in*

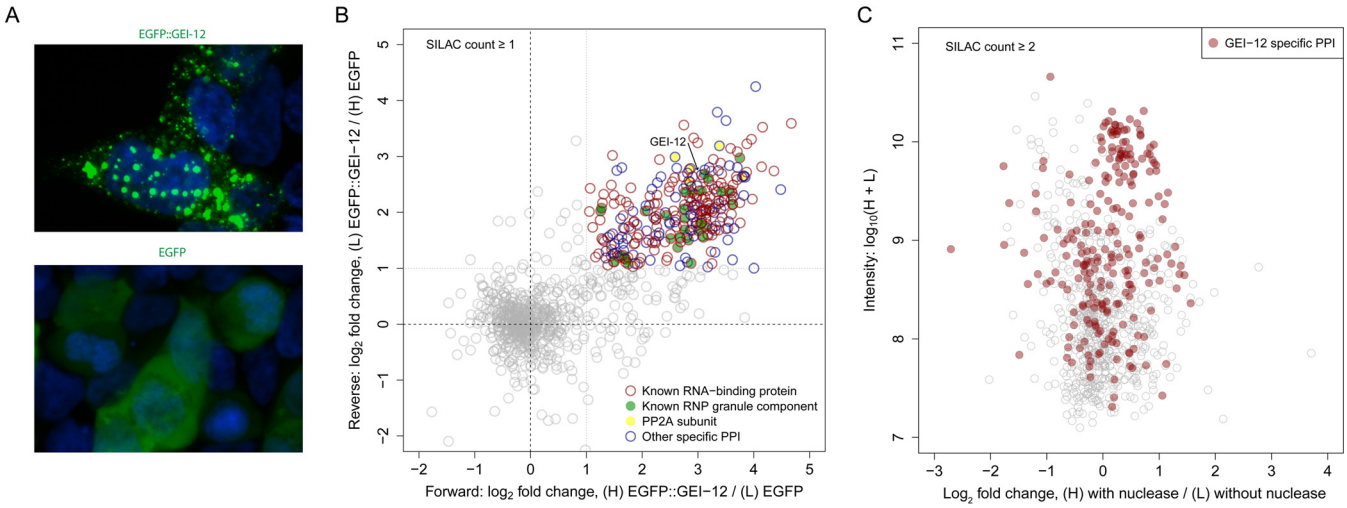

FIG. 7. **GEI-12 forms granules in mammalian cells and interacts with RNA-binding proteins and PP2A.** *A*, EGFP::GEI-12 expressed in HEK293T cells forms granules (top), whereas control cells expressing EGFP only do not (bottom). DAPI staining shown in blue. *B*, Label-swap SILAC pull-downs of EGFP::GEI-12 in HEK293T cells. The majority of interacting proteins are annotated with the GO term "RNA binding". Other interactors include known RNP granule components and multiple PP2A subunits (catalytic subunit, structural subunits, and several regulatory subunit B56 subfamily members). *C*, SILAC pull-down of EGFP::GEI-12 in HEK293T lysates comparing with (H) and without (L) nuclease pre-treatment. The majority of GEI-12 interactions remained unaltered upon nuclease treatment, suggesting that they are not RNA dependent.

vivo interactome (IVI) during *C. elegans* embryogenesis. Despite the limited scale, our unbiased data contain several previously described interactions and thus reflect known biology. More importantly, the high fraction of shared RNAi phenotypes among interaction partners demonstrates that our network also predicts protein function.

The comparison with yeast two-hybrid studies indicates that our *in vivo* interactome mapping approach provides data with higher functional relevance. As with any experimental approach, however, it is important to be cognizant of technical limitations. Most importantly, GFP-fusion proteins may be expressed at different levels and/or may not fully recapitulate the functions of their endogenous counterparts. Although the first issue can be addressed by expressing transgenes under endogenous *cis* regulatory control (77), the GFP tag—like any other tag—might still affect *in vivo* protein function. Using transgenes that can rescue loss-of-function phenotypes should help to minimize this caveat. Next, the potential introduction of artifacts during biochemical purification could be limited by crosslinking samples *in situ* prior to lysis; even though our controls indicated that post-lysis interactions were negligible in at least one test case, we cannot rule out the possibility that some post-lysis PPIs may be recovered in assays with different fusion proteins. Finally, our current IVI mapping strategy is relatively low throughput because we perform experiments using one bait protein at a time. This may not be a major limitation in practice, given the fact that we generated interaction data for almost 500 proteins using pull-down experiments with only eight bait proteins. This might be because of the central function these proteins play in embryogenesis. Performing similar experiments with ~100 selected "hub" baits would probably cover a substantial fraction of the worm interactome. It is possible to envision future improvements to IVI mapping approaches that would enable the simultaneous interrogation of multiple bait proteins, which could significantly enhance throughput.

RNP granules have emerged as important players in the post-transcriptional regulation of gene expression in many organisms (78). Like other membraneless compartments, or organelles, they resemble liquids that form by phase separation from the cytoplasm (79, 80). *C. elegans* P granules are probably the most extensively characterized *in vivo* model for RNP granules (12). Although genetic analysis has placed several P granule components into an assembly pathway (DEPS-1 → GLH-1 → PGL-1/3 → IFE-1), the cellular signaling events that mediate granule formation are still incompletely understood. Time-lapse microscopy has shown that localization occurs via condensation of the liquid-like P granules at the posterior and dissolution at the anterior (13). Dissolution correlates with the levels of the polarity protein MEX-5, which is concentrated in the anterior of the one-cell embryo, suggesting that MEX-5 promotes the posterior localization of P granules by promoting their dissolution in the anterior. The activity of MEX-5 and the closely related MEX-6 are regulated by polo-like kinases (PLK-1/2), and this interaction is strongly enhanced by MBK-2 as the priming kinase (81). On the other hand, PPTR-1, a regulatory subunit of the protein phosphatase PP2A, is specifically required for embryonic P granule assembly during mitosis (75). These data indicate that P granule dynamics are regulated by the interplay of kinases (MBK-2, PLK-1/2) and phosphatases (PP2A/PPTR-1), but how these activities are coordinated mechanistically is unclear.

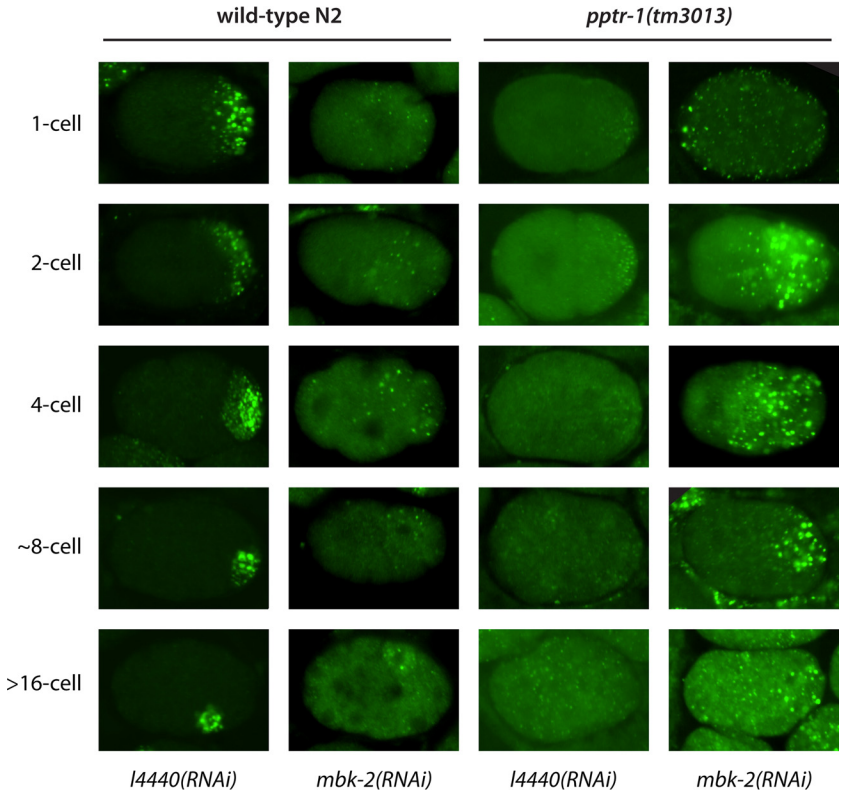

FIG. 8. **Depletion of *mbk-2* by RNAi restores P granule formation in *pptr-1* mutant embryos.** P granules do not segregate normally to the posterior because of loss of cell polarity upon *mbk-2* depletion. Knocking down *mbk-2* leads to missegregation of P granules in wild-type N2 embryos. *L4440(RNAi)* served as control.

Here, we identified GEI-12 and its paralog as novel regulators of P granule dynamics and germline competence. First, we found that GEI-12 co-purified with MBK-2 and PPTR-2. Second, we observed that the protein localizes to the P lineage and is required for granule assembly and maintenance of the germline. Third, we found that GEI-12 forms granules in mammalian cells and interacts with RNA binding proteins and PP2A family proteins. Finally, we observed that knocking down *mbk-2* restores P granule formation in the *pptr-1* mutant. Recently, binding between GEI-12 and PPTR-1, the loss-of-function phenotypes of *gei-12* in P granule assembly and fertility, and the suppression of *pptr-1* mutant phenotype by *mbk-2(RNAi)* were also independently reported by Wang *et al.* (25). In addition, we show that GEI-12, MBK-2, and PPTR-2 physically interact and that GEI-12 forms granules in mammalian cells.

The emerging model from our study is that P granule assembly and disassembly may be regulated by dephosphorylation and phosphorylation, respectively, of GEI-12 and its paralog. In this scenario, unphosphorylated GEI-12 may serve as a scaffold for the assembly of additional P granule components. Nonetheless, despite the physical and genetic interaction data, the current study lacks direct evidence to demonstrate a kinase/phosphatase/substrate relation. Recent findings from the Seydoux lab (25) revealed that MBK-2 can phosphorylate GEI-12 *in vitro*, and that the *in vivo* phosphorylation level of the protein is affected by MBK-2 and PPTR-1. In addition, we show that (1) MBK-2 physically interacts with both GEI-12 and PPTR-2, and (2) GEI-12 forms granules when expressed in mammalian cells. Our finding that granules induced by GEI-12 in mammalian cells are rich in known RNP granule components, and that they also contain catalytic, structural and regulatory subunits of the PP2A family of phosphatases, suggest that the fundamental mechanisms of granule assembly are conserved between worms and humans. It would therefore be very interesting to test if PP2A stabilizes RNP granules in mammals. Coupled with the fact that GEI-12 has no obvious mammalian counterparts, but that it is rich in low complexity (LC) regions and potential serine/threonine phosphorylation sites (nearly 20% of residues in GEI-12 are Ser or Thr), it is possible that RNP granule formation *in vivo* is regulated by bulk biochemical properties of these aggregates rather than sequence-specific molecular interactions. Because of the highly negatively charged nature of RNA, it would thus be expected that dissolution of RNP granules would be driven by state transitions between lowly and highly phosphorylated forms of putative scaffold proteins like GEI-12. This idea is fully consistent with previous discoveries on the liquid-like behavior of RNP granules and the ability of LC-rich proteins to form spontaneous aggregates in solution (13, 72).

In summary, our data show that *in vivo* interaction proteomics provides unique insights into animal development. The *in vivo* nature of this approach also produces data with a higher functional relevance than classical methods. Although a major strength of *C. elegans* has traditionally been its utility for genetic analysis, our work demonstrates that this model or-

ganism is also well suited for systematic biochemical analysis of protein-protein interactions. Combined with the recent generation of genome-wide collections of GFP fusion constructs (77), we expect the quantitative approach using *C. elegans* embryos to become a valuable orthogonal tool both to uncover new biology and to deepen our understanding of universal mechanistic principles using this animal model system.

Acknowledgements—We would like to thank Florian Paul (MDC) for contribution during the early stage of the project. We thank Olivia Bay (NYU), Katherine Erickson (NYU), Martha Hergeselle (MDC), Jessica Lucas (NYU), Noah Smit (NYU) and Christian Sommer (MDC) for excellent technical assistance, Kahn Rhrissorrakrai (IBM) for helpful discussions on protein network analysis, and Henrik Zauber (MDC) for help with generating annotated MS/MS spectra. We would also like to thank Miyeko Mana (NYU), Shohei Mitani (Tokyo Women's Medical Univ.), Nikolaus Rajewsky (MDC) and the Caenorhabditis Genetics Center for providing strains. The Developmental Studies Hybridoma Bank, Peter Boag (Monash Univ.) and Nancy Huang (Colorado College) kindly provided antibodies. We also thank Markus Landthaler (MDC), Florian Paul (MDC) and Sean West (NYU) for reagents and plasmids.

* This work was supported by NIH grant R01 HD046236 (to FP and KCG) and the Helmholtz Association (to MS). JXC received funding from the MDC-NYU PhD exchange program, supported by the BMBF (0315362) and the Berlin Institute for Medical Systems Biology (BIMSB). The content is solely the responsibility of the authors and does not necessarily represent the official views of the National Institutes of Health.

S This article contains supplemental material.

‡‡ To whom correspondence should be addressed: Max Delbrück Center for Molecular Medicine, Robert-Rössle-Str. 10, D-13092 Berlin, Germany. Tel.: +49 30 9406 3574, Fax: +49 30 9406 2394, E-mail: matthias.selbach@mdc-berlin.de; Kristin C. Gunsalus, Center for Genomics and Systems Biology, Department of Biology, New York University, 12 Waverly Place, 8th Floor, New York, NY 10003. Email: kcg1@nyu.edu.

Author Contributions: JXC, FP, KCG and MS conceived and designed the study. JXC, PGC, DM and JP performed experiments. JXC, PGC, JP, FP, KCG and MS analyzed and interpreted the data. FP, KCG and MS supervised the study. JXC, PGC, FP, KCG and MS wrote the article.

Conflict of Interest: The authors declare that there are no conflicts of interest.

REFERENCES

1. Malovannaya, A., Lanz, R. B., Jung, S. Y., Bulynko, Y., Le, N. T., Chan, D. W., Ding, C., Shi, Y., Yucer, N., Krenciute, G., Kim, B. J., Li, C., Chen, R., Li, W., Wang, Y., O'Malley, B. W., and Qin, J. (2011) Analysis of the human endogenous coregulator complexome. *Cell* **145,** 787–799
2. Rual, J. F., Venkatesan, K., Hao, T., Hirozane-Kishikawa, T., Dricot, A., Li, N., Berriz, G. F., Gibbons, F. D., Dreze, M., Ayivi-Guedehoussou, N., Klitgord, N., Simon, C., Boxem, M., Milstein, S., Rosenberg, J., Goldberg, D. S., Zhang, L. V., Wong, S. L., Franklin, G., Li, S., Albala, J. S., Lim, J., Fraughton, C., Llamosas, E., Cevik, S., Bex, C., Lamesch, P., Sikorski, R. S., Vandenhaute, J., Zoghbi, H. Y., Smolyar, A., Bosak, S., Sequerra, R., Doucette-Stamm, L., Cusick, M. E., Hill, D. E., Roth, F. P., and Vidal, M. (2005) Towards a proteome-scale map of the human protein-protein interaction network. *Nature* **437,** 1173–1178
3. Li, S., Armstrong, C. M., Bertin, N., Ge, H., Milstein, S., Boxem, M., Vidalain, P. O., Han, J. D., Chesneau, A., Hao, T., Goldberg, D. S., Li, N., Martinez, M., Rual, J. F., Lamesch, P., Xu, L., Tewari, M., Wong, S. L., Zhang, L. V., Berriz, G. F., Jacotot, L., Vaglio, P., Reboul, J., Hirozane-Kishikawa, T., Li, Q., Gabel, H. W., Elewa, A., Baumgartner, B., Rose, D. J., Yu, H., Bosak, S., Sequerra, R., Fraser, A., Mango, S. E., Saxton, W. M., Strome, S., Van Den Heuvel, S., Piano, F., Vandenhaute, J., Sardet, C., Gerstein, M., Doucette-Stamm, L., Gunsalus, K. C., Harper, J. W., Cusick, M. E., Roth, F. P., Hill, D. E., and Vidal, M. (2004) A map of the interactome network of the metazoan C. elegans. *Science* **303,** 540–543
4. Boxem, M., Maliga, Z., Klitgord, N., Li, N., Lemmens, I., Mana, M., de Lichtervelde, L., Mul, J. D., van de Peut, D., Devos, M., Simonis, N., Yildirim, M. A., Cokol, M., Kao, H. L., de Smet, A. S., Wang, H., Schlaitz, A. L., Hao, T., Milstein, S., Fan, C., Tipsword, M., Drew, K., Galli, M., Rhrissorrakrai, K., Drechsel, D., Koller, D., Roth, F. P., Iakoucheva, L. M., Dunker, A. K., Bonneau, R., Gunsalus, K. C., Hill, D. E., Piano, F., Tavernier, J., van den Heuvel, S., Hyman, A. A., and Vidal, M. (2008) A protein domain-based interactome network for C. elegans early embryogenesis. *Cell* **134,** 534–545
5. Stelzl, U., Worm, U., Lalowski, M., Haenig, C., Brembeck, F. H., Goehler, H., Stroedicke, M., Zenkner, M., Schoenherr, A., Koeppen, S., Timm, J., Mintzlaff, S., Abraham, C., Bock, N., Kietzmann, S., Goedde, A., Toksoz, E., Droege, A., Krobitsch, S., Korn, B., Birchmeier, W., Lehrach, H., and Wanker, E. E. (2005) A human protein-protein interaction network: a resource for annotating the proteome. *Cell* **122,** 957–968
6. Simonis, N., Rual, J. F., Carvunis, A. R., Tasan, M., Lemmens, I., Hirozane-Kishikawa, T., Hao, T., Sahalie, J. M., Venkatesan, K., Gebreab, F., Cevik, S., Klitgord, N., Fan, C., Braun, P., Li, N., Ayivi-Guedehoussou, N., Dann, E., Bertin, N., Szeto, D., Dricot, A., Yildirim, M. A., Lin, C., de Smet, A. S., Kao, H. L., Simon, C., Smolyar, A., Ahn, J. S., Tewari, M., Boxem, M., Milstein, S., Yu, H., Dreze, M., Vandenhaute, J., Gunsalus, K. C., Cusick, M. E., Hill, D. E., Tavernier, J., Roth, F. P., and Vidal, M. (2009) Empirically controlled mapping of the Caenorhabditis elegans protein-protein interactome network. *Nat. Methods* **6,** 47–54
7. Gavin, A. C., Bosche, M., Krause, R., Grandi, P., Marzioch, M., Bauer, A., Schultz, J., Rick, J. M., Michon, A. M., Cruciat, C. M., Remor, M., Hofert, C., Schelder, M., Brajenovic, M., Ruffner, H., Merino, A., Klein, K., Hudak, M., Dickson, D., Rudi, T., Gnau, V., Bauch, A., Bastuck, S., Huhse, B., Leutwein, C., Heurtier, M. A., Copley, R. R., Edelmann, A., Querfurth, E., Rybin, V., Drewes, G., Raida, M., Bouwmeester, T., Bork, P., Seraphin, B., Kuster, B., Neubauer, G., and Superti-Furga, G. (2002) Functional organization of the yeast proteome by systematic analysis of protein complexes. *Nature* **415,** 141–147
8. Ewing, R. M., Chu, P., Elisma, F., Li, H., Taylor, P., Climie, S., McBroom-Cerajewski, L., Robinson, M. D., O'Connor, L., Li, M., Taylor, R., Dharsee, M., Ho, Y., Heilbut, A., Moore, L., Zhang, S., Ornatsky, O., Bukhman, Y. V., Ethier, M., Sheng, Y., Vasilescu, J., Abu-Farha, M., Lambert, J. P., Duewel, H. S., Stewart, II, Kuehl, B., Hogue, K., Colwill, K., Gladwish, K., Muskat, B., Kinach, R., Adams, S. L., Moran, M. F., Morin, G. B., Topaloglou, T., and Figeys, D. (2007) Large-scale mapping of human protein-protein interactions by mass spectrometry. *Mol. Systems Biol.* **3,** 89
9. Gingras, A. C., Gstaiger, M., Raught, B., and Aebersold, R. (2007) Analysis of protein complexes using mass spectrometry. *Nat. Rev. Mol. Cell Biol.* **8,** 645–654
10. Suzuki, A., and Ohno, S. (2006) The PAR-aPKC system: lessons in polarity. *J. Cell Sci.* **119,** 979–987
11. Hoege, C., and Hyman, A. A. (2013) Principles of PAR polarity in Caenorhabditis elegans embryos. *Nat. Rev. Mol. Cell Biol.* **14,** 315–322
12. Updike, D., and Strome, S. (2010) P granule assembly and function in Caenorhabditis elegans germ cells. *J. Androl.* **31,** 53–60
13. Brangwynne, C. P., Eckmann, C. R., Courson, D. S., Rybarska, A., Hoege, C., Gharakhani, J., Julicher, F., and Hyman, A. A. (2009) Germline P granules are liquid droplets that localize by controlled dissolution/condensation. *Science* **324,** 1729–1732
14. Zanin, E., Dumont, J., Gassmann, R., Cheeseman, I., Maddox, P., Bahmanyar, S., Carvalho, A., Niessen, S., Yates, J. R., 3rd, Oegema, K., and Desai, A. (2011) Affinity purification of protein complexes in C. elegans. *Methods Cell Biol.* **106,** 289–322
15. Cheeseman, I. M., Niessen, S., Anderson, S., Hyndman, F., Yates, J. R., 3rd, Oegema, K., and Desai, A. (2004) A conserved protein network controls assembly of the outer kinetochore and its ability to sustain tension. *Genes Develop.* **18,** 2255–2268
16. Lowe, N., Rees, J. S., Roote, J., Ryder, E., Armean, I. M., Johnson, G., Drummond, E., Spriggs, H., Drummond, J., Magbanua, J. P., Naylor, H., Sanson, B., Bastock, R., Huelsmann, S., Trovisco, V., Landgraf, M.,

Knowles-Barley, S., Armstrong, J. D., White-Cooper, H., Hansen, C., Phillips, R. G., Consortium, U. K. D. P. T. S., Lilley, K. S., Russell, S., and St Johnston, D. (2014) Analysis of the expression patterns, subcellular localisations and interaction partners of Drosophila proteins using a pigP protein trap library. *Development* **141,** 3994–4005

17. Angrand, P. O., Segura, I., Volkel, P., Ghidelli, S., Terry, R., Brajenovic, M., Vintersten, K., Klein, R., Superti-Furga, G., Drewes, G., Kuster, B., Bouwmeester, T., and Acker-Palmer, A. (2006) Transgenic mouse proteomics identifies new 14–3-3-associated proteins involved in cytoskeletal rearrangements and cell signaling. *Mol. Cell. Proteomics* **5,** 2211–2227
18. Bartoi, T., Rigbolt, K. T., Du, D., Kohr, G., Blagoev, B., and Kornau, H. C. (2010) GABAB receptor constituents revealed by tandem affinity purification from transgenic mice. *J. Biol. Chem.* **285,** 20625–20633
19. Paul, F. E., Hosp, F., and Selbach, M. (2011) Analyzing protein-protein interactions by quantitative mass spectrometry. *Methods* **54,** 387–395
20. Vermeulen, M., Hubner, N. C., and Mann, M. (2008) High confidence determination of specific protein-protein interactions using quantitative mass spectrometry. *Current Opinion Biotechno.y* **19,** 331–337
21. Meyer, K., and Selbach, M. (2015) Quantitative affinity purification mass spectrometry: a versatile technology to study protein-protein interactions. *Frontiers Genetics* **6,** 237
22. Hubner, N. C., Bird, A. W., Cox, J., Splettstoesser, B., Bandilla, P., Poser, I., Hyman, A., and Mann, M. (2010) Quantitative proteomics combined with BAC TransgeneOmics reveals in vivo protein interactions. *J. Cell Biol.* **189,** 739–754
23. Hanack, C., Moroni, M., Lima, W. C., Wende, H., Kirchner, M., Adelfinger, L., Schrenk-Siemens, K., Tappe-Theodor, A., Wetzel, C., Kuich, P. H., Gassmann, M., Roggenkamp, D., Bettler, B., Lewin, G. R., Selbach, M., and Siemens, J. (2015) GABA Blocks Pathological but Not Acute TRPV1 Pain Signals. *Cell* **160,** 759–770
24. Andlauer, T. F., Scholz-Kornehl, S., Tian, R., Kirchner, M., Babikir, H. A., Depner, H., Loll, B., Quentin, C., Gupta, V. K., Holt, M. G., Dipt, S., Cressy, M., Wahl, M. C., Fiala, A., Selbach, M., Schwarzel, M., and Sigrist, S. J. (2014) Drep-2 is a novel synaptic protein important for learning and memory. *eLife* **3,** e03895
25. Wang, J. T., Smith, J., Chen, B., Schmidt, H., Rasoloson, D., Paix, A., Lambrus, B. G., Calidas, D., Betzig, E., and Seydoux, G. (2014) Regulation of RNA granule dynamics by phosphorylation of serine-rich, intrinsically-disordered proteins in. *eLife* **3,** e04591
26. Brenner, S. (1974) The genetics of Caenorhabditis elegans. *Genetics* **77,** 71–94
27. Stoeckius, M., Grun, D., Kirchner, M., Ayoub, S., Torti, F., Piano, F., Herzog, M., Selbach, M., and Rajewsky, N. (2014) Global characterization of the oocyte-to-embryo transition in Caenorhabditis elegans uncovers a novel mRNA clearance mechanism. *EMBO J.* **33,** 1751–1766
28. Jungkamp, A. C., Stoeckius, M., Mecenas, D., Grun, D., Mastrobuoni, G., Kempa, S., and Rajewsky, N. (2011) In vivo and transcriptome-wide identification of RNA binding protein target sites. *Mol. Cell* **44,** 828–840
29. Raich, W. B., Moorman, C., Lacefield, C. O., Lehrer, J., Bartsch, D., Plasterk, R. H., Kandel, E. R., and Hobert, O. (2003) Characterization of Caenorhabditis elegans homologs of the Down syndrome candidate gene DYRK1A. *Genetics* **163,** 571–580
30. Pellettieri, J., Reinke, V., Kim, S. K., and Seydoux, G. (2003) Coordinate activation of maternal protein degradation during the egg-to-embryo transition in C. elegans. *Developmental Cell* **5,** 451–462
31. Merritt, C., Rasoloson, D., Ko, D., and Seydoux, G. (2008) 3′ UTRs are the primary regulators of gene expression in the C. elegans germline. *Current Biol.* **18,** 1476–1482
32. Voronina, E., and Seydoux, G. (2010) The C. elegans homolog of nucleoporin Nup98 is required for the integrity and function of germline P granules. *Development* **137,** 1441–1450
33. Kaitna, S., Mendoza, M., Jantsch-Plunger, V., and Glotzer, M. (2000) Incenp and an aurora-like kinase form a complex essential for chromosome segregation and efficient completion of cytokinesis. *Current Biol.* **10,** 1172–1181
34. Cheeks, R. J., Canman, J. C., Gabriel, W. N., Meyer, N., Strome, S., and Goldstein, B. (2004) C. elegans PAR proteins function by mobilizing and stabilizing asymmetrically localized protein complexes. *Current Biol.* **14,** 851–862
35. Schonegg, S., Constantinescu, A. T., Hoege, C., and Hyman, A. A. (2007) The Rho GTPase-activating proteins RGA-3 and RGA-4 are required to set the initial size of PAR domains in Caenorhabditis elegans one-cell embryos. *Proc. Natl. Acad. Sci. U. S. A.* **104,** 14976–14981
36. Zeiser, E., Frokjaer-Jensen, C., Jorgensen, E., and Ahringer, J. (2011) MosSCI and gateway compatible plasmid toolkit for constitutive and inducible expression of transgenes in the C. elegans germline. *PloS One* **6,** e20082
37. Fraser, A. G., Kamath, R. S., Zipperlen, P., Martinez-Campos, M., Sohrmann, M., and Ahringer, J. (2000) Functional genomic analysis of C. elegans chromosome I by systematic RNA interference. *Nature* **408,** 325–330
38. Kamath, R. S., Martinez-Campos, M., Zipperlen, P., Fraser, A. G., and Ahringer, J. (2001) Effectiveness of specific RNA-mediated interference through ingested double-stranded RNA in Caenorhabditis elegans. *Genome Biol.* **2**, RESEARCH0002
39. Takeda, K., Watanabe, C., Qadota, H., Hanazawa, M., and Sugimoto, A. (2008) Efficient production of monoclonal antibodies recognizing specific structures in Caenorhabditis elegans embryos using an antigen subtraction method. *Genes Cells* **13,** 653–665
40. Strome, S., and Wood, W. B. (1983) Generation of asymmetry and segregation of germ-line granules in early C. elegans embryos. *Cell* **35,** 15–25
41. Schneider, C. A., Rasband, W. S., and Eliceiri, K. W. (2012) NIH Image to ImageJ: 25 years of image analysis. *Nat. Methods* **9,** 671–675
42. Cox, J., and Mann, M. (2008) MaxQuant enables high peptide identification rates, individualized p.p.b.-range mass accuracies and proteome-wide protein quantification. *Nat. Biotechnol.* **26,** 1367–1372
43. Cox, J., Neuhauser, N., Michalski, A., Scheltema, R. A., Olsen, J. V., and Mann, M. (2011) Andromeda: a peptide search engine integrated into the MaxQuant environment. *J. Proteome Res.* **10,** 1794–1805
44. Cox, J., Hein, M. Y., Luber, C. A., Paron, I., Nagaraj, N., and Mann, M. (2014) Accurate proteome-wide label-free quantification by delayed normalization and maximal peptide ratio extraction, termed MaxLFQ. *Mol. Cell. Proteomics* **13,** 2513–2526
45. Tusher, V. G., Tibshirani, R., and Chu, G. (2001) Significance analysis of microarrays applied to the ionizing radiation response. *Proc. Natl. Acad. Sci. U.S.A.* **98,** 5116–5121
46. Li, W. (2012) Volcano plots in analyzing differential expressions with mRNA microarrays. *J. Bioinformatics Computational Biol.* **10**, 1231003
47. Boag, P. R., Nakamura, A., and Blackwell, T. K. (2005) A conserved RNA-protein complex component involved in physiological germline apoptosis regulation in C. elegans. *Development* **132,** 4975–4986
48. Sengupta, M. S., Low, W. Y., Patterson, J. R., Kim, H. M., Traven, A., Beilharz, T. H., Colaiacovo, M. P., Schisa, J. A., and Boag, P. R. (2013) ifet-1 is a broad-scale translational repressor required for normal P granule formation in C. elegans. *J. Cell Sci.* **126,** 850–859
49. Huang, N. N., Mootz, D. E., Walhout, A. J., Vidal, M., and Hunter, C. P. (2002) MEX-3 interacting proteins link cell polarity to asymmetric gene expression in Caenorhabditis elegans. *Development* **129,** 747–759
50. Falcon, S., and Gentleman, R. (2007) Using GOstats to test gene lists for GO term association. *Bioinformatics* **23,** 257–258
51. Boag, P. R., Atalay, A., Robida, S., Reinke, V., and Blackwell, T. K. (2008) Protection of specific maternal messenger RNAs by the P body protein CGH-1 (Dhh1/RCK) during Caenorhabditis elegans oogenesis. *J. Cell Biol.* **182,** 543–557
52. Audhya, A., Hyndman, F., McLeod, I. X., Maddox, A. S., Yates, J. R., 3rd, Desai, A., and Oegema, K. (2005) A complex containing the Sm protein CAR-1 and the RNA helicase CGH-1 is required for embryonic cytokinesis in Caenorhabditis elegans. *J. Cell Biol.* **171,** 267–279
53. Squirrell, J. M., Eggers, Z. T., Luedke, N., Saari, B., Grimson, A., Lyons, G. E., Anderson, P., and White, J. G. (2006) CAR-1, a protein that localizes with the mRNA decapping component DCAP-1, is required for cytokinesis and ER organization in Caenorhabditis elegans embryos. *Mol. Biol. Cell* **17,** 336–344
54. Lee, M. H., and Schedl, T. (2010) C. elegans star proteins, GLD-1 and ASD-2, regulate specific RNA targets to control development. *Adv. Exp. Med. Biol.* **693,** 106–122
55. Scheckel, C., Gaidatzis, D., Wright, J. E., and Ciosk, R. (2012) Genome-wide analysis of GLD-1-mediated mRNA regulation suggests a role in mRNA storage. *PLoS Genetics* **8**, e1002742
56. Hoege, C., Constantinescu, A. T., Schwager, A., Goehring, N. W., Kumar, P., and Hyman, A. A. (2010) LGL can partition the cortex of one-cell Caenorhabditis elegans embryos into two domains. *Current Biol.* **20,** 1296–1303

57. Mishima, M., Kaitna, S., and Glotzer, M. (2002) Central spindle assembly and cytokinesis require a kinesin-like protein/RhoGAP complex with microtubule bundling activity. *Developmental Cell* **2,** 41–54
58. Tian, Y., Li, Z., Hu, W., Ren, H., Tian, E., Zhao, Y., Lu, Q., Huang, X., Yang, P., Li, X., Wang, X., Kovacs, A. L., Yu, L., and Zhang, H. (2010) C. elegans screen identifies autophagy genes specific to multicellular organisms. *Cell* **141,** 1042–1055
59. Zhang, Y., Yan, L., Zhou, Z., Yang, P., Tian, E., Zhang, K., Zhao, Y., Li, Z., Song, B., Han, J., Miao, L., and Zhang, H. (2009) SEPA-1 mediates the specific recognition and degradation of P granule components by autophagy in C. elegans. *Cell* **136,** 308–321
60. Fraser, H. B., and Plotkin, J. B. (2007) Using protein complexes to predict phenotypic effects of gene mutation. *Genome Biol.* **8,** R252
61. Sonnichsen, B., Koski, L. B., Walsh, A., Marschall, P., Neumann, B., Brehm, M., Alleaume, A. M., Artelt, J., Bettencourt, P., Cassin, E., Hewitson, M., Holz, C., Khan, M., Lazik, S., Martin, C., Nitzsche, B., Ruer, M., Stamford, J., Winzi, M., Heinkel, R., Roder, M., Finell, J., Hantsch, H., Jones, S. J., Jones, M., Piano, F., Gunsalus, K. C., Oegema, K., Gonczy, P., Coulson, A., Hyman, A. A., and Echeverri, C. J. (2005) Full-genome RNAi profiling of early embryogenesis in Caenorhabditis elegans. *Nature* **434,** 462–469
62. Voronina, E., Seydoux, G., Sassone-Corsi, P., and Nagamori, I. (2011) RNA granules in germ cells. *Cold Spring Harbor Perspectives Biol.* **3,** a002774
63. Robertson, S., and Lin, R. (2013) The oocyte-to-embryo transition. *Adv. Exp. Med. Biol.* **757,** 351–372
64. Updike, D. L., and Strome, S. (2009) A genomewide RNAi screen for genes that affect the stability, distribution and function of P granules in Caenorhabditis elegans. *Genetics* **183,** 1397–1419
65. Maruyama, R., Velarde, N. V., Klancer, R., Gordon, S., Kadandale, P., Parry, J. M., Hang, J. S., Rubin, J., Stewart-Michaelis, A., Schweinsberg, P., Grant, B. D., Piano, F., Sugimoto, A., and Singson, A. (2007) EGG-3 regulates cell-surface and cortex rearrangements during egg activation in Caenorhabditis elegans. *Current Biol.* **17,** 1555–1560
66. Stitzel, M. L., Cheng, K. C., and Seydoux, G. (2007) Regulation of MBK-2/Dyrk kinase by dynamic cortical anchoring during the oocyte-to-zygote transition. *Current Biol.* **17,** 1545–1554
67. Cheng, K. C., Klancer, R., Singson, A., and Seydoux, G. (2009) Regulation of MBK-2/DYRK by CDK-1 and the pseudophosphatases EGG-4 and EGG-5 during the oocyte-to-embryo transition. *Cell* **139,** 560–572
68. Zhang, Y., Foster, J. M., Nelson, L. S., Ma, D., and Carlow, C. K. (2005) The chitin synthase genes chs-1 and chs-2 are essential for C. elegans development and responsible for chitin deposition in the eggshell and pharynx, respectively. *Developmental Biol.* **285,** 330–339
69. Kawasaki, I., Shim, Y. H., Kirchner, J., Kaminker, J., Wood, W. B., and Strome, S. (1998) PGL-1, a predicted RNA-binding component of germ granules, is essential for fertility in C. elegans. *Cell* **94,** 635–645
70. Updike, D. L., Knutson, A. K., Egelhofer, T. A., Campbell, A. C., and Strome, S. (2014) Germ-granule components prevent somatic development in the C. elegans germline. *Current Biol.* **24,** 970–975
71. Leacock, S. W., and Reinke, V. (2008) MEG-1 and MEG-2 are embryo-specific P-granule components required for germline development in Caenorhabditis elegans. *Genetics* **178,** 295–306
72. Kato, M., Han, T. W., Xie, S., Shi, K., Du, X., Wu, L. C., Mirzaei, H., Goldsmith, E. J., Longgood, J., Pei, J., Grishin, N. V., Frantz, D. E., Schneider, J. W., Chen, S., Li, L., Sawaya, M. R., Eisenberg, D., Tycko, R., and McKnight, S. L. (2012) Cell-free formation of RNA granules: low complexity sequence domains form dynamic fibers within hydrogels. *Cell* **149,** 753–767
73. Hanazawa, M., Yonetani, M., and Sugimoto, A. (2011) PGL proteins self associate and bind RNPs to mediate germ granule assembly in C. elegans. *J. Cell Biol.* **192,** 929–937
74. Wippich, F., Bodenmiller, B., Trajkovska, M. G., Wanka, S., Aebersold, R., and Pelkmans, L. (2013) Dual specificity kinase DYRK3 couples stress granule condensation/dissolution to mTORC1 signaling. *Cell* **152,** 791–805
75. Gallo, C. M., Wang, J. T., Motegi, F., and Seydoux, G. (2010) Cytoplasmic partitioning of P granule components is not required to specify the germline in C. elegans. *Science* **330,** 1685–1689
76. Lundby, A., Rossin, E. J., Steffensen, A. B., Acha, M. R., Newton-Cheh, C., Pfeufer, A., Lynch, S. N., Consortium, Q. T. I. I. G., Olesen, S. P., Brunak, S., Ellinor, P. T., Jukema, J. W., Trompet, S., Ford, I., Macfarlane, P. W., Krijthe, B. P., Hofman, A., Uitterlinden, A. G., Stricker, B. H., Nathoe, H. M., Spiering, W., Daly, M. J., Asselbergs, F. W., van der Harst, P., Milan, D. J., de Bakker, P. I., Lage, K., and Olsen, J. V. (2014) Annotation of loci from genome-wide association studies using tissue-specific quantitative interaction proteomics. *Nat. Methods* **11,** 868–874
77. Sarov, M., Murray, J. I., Schanze, K., Pozniakovski, A., Niu, W., Angermann, K., Hasse, S., Rupprecht, M., Vinis, E., Tinney, M., Preston, E., Zinke, A., Enst, S., Teichgraber, T., Janette, J., Reis, K., Janosch, S., Schloissnig, S., Ejsmont, R. K., Slightam, C., Xu, X., Kim, S. K., Reinke, V., Stewart, A. F., Snyder, M., Waterston, R. H., and Hyman, A. A. (2012) A genome-scale resource for in vivo tag-based protein function exploration in C. elegans. *Cell* **150,** 855–866
78. Anderson, P., and Kedersha, N. (2006) RNA granules. *J. Cell Biol.* **172,** 803–808
79. Hyman, A. A., Weber, C. A., and Julicher, F. (2014) Liquid-liquid phase separation in biology. *Annu. Rev. Cell Dev. Biol.* **30,** 39–58
80. Li, P., Banjade, S., Cheng, H. C., Kim, S., Chen, B., Guo, L., Llaguno, M., Hollingsworth, J. V., King, D. S., Banani, S. F., Russo, P. S., Jiang, Q. X., Nixon, B. T., and Rosen, M. K. (2012) Phase transitions in the assembly of multivalent signalling proteins. *Nature* **483,** 336–340
81. Nishi, Y., Rogers, E., Robertson, S. M., and Lin, R. (2008) Polo kinases regulate C. elegans embryonic polarity via binding to DYRK2-primed MEX-5 and MEX-6. *Development* **135,** 687–697
82. Wootton, J. C., and Federhen, S. (1996) Analysis of compositionally biased regions in sequence databases. *Methods Enzymol.* **266,** 554–571